

Engineering Technology Reports, Volume 2: Technology Base FY01

C. Minichino, D. Meeker

July 1, 2002

U.S. Department of Energy

Lawrence
Livermore
National
Laboratory

DISCLAIMER

This document was prepared as an account of work sponsored by an agency of the United States Government. Neither the United States Government nor the University of California nor any of their employees, makes any warranty, express or implied, or assumes any legal liability or responsibility for the accuracy, completeness, or usefulness of any information, apparatus, product, or process disclosed, or represents that its use would not infringe privately owned rights. Reference herein to any specific commercial product, process, or service by trade name, trademark, manufacturer, or otherwise, does not necessarily constitute or imply its endorsement, recommendation, or favoring by the United States Government or the University of California. The views and opinions of authors expressed herein do not necessarily state or reflect those of the United States Government or the University of California, and shall not be used for advertising or product endorsement purposes.

This is a preprint of a paper intended for publication in a journal or proceedings. Since changes may be made before publication, this preprint is made available with the understanding that it will not be cited or reproduced without the permission of the author.

This report has been reproduced directly from the best available copy.

Available electronically at <http://www.doc.gov/bridge>

Available for a processing fee to U.S. Department of Energy
And its contractors in paper from
U.S. Department of Energy
Office of Scientific and Technical Information
P.O. Box 62
Oak Ridge, TN 37831-0062
Telephone: (865) 576-8401
Facsimile: (865) 576-5728
E-mail: reports@adonis.osti.gov

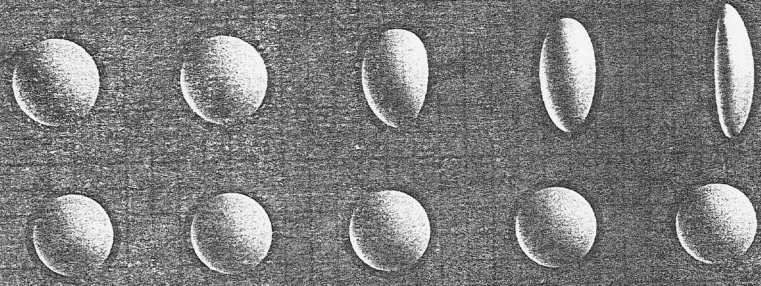
Available for the sale to the public from
U.S. Department of Commerce
National Technical Information Service
5285 Port Royal Road
Springfield, VA 22161
Telephone: (800) 553-6847
Facsimile: (703) 605-6900
E-mail: orders@ntis.fedworld.gov
Online ordering: <http://www.ntis.gov/ordering.htm>

OR

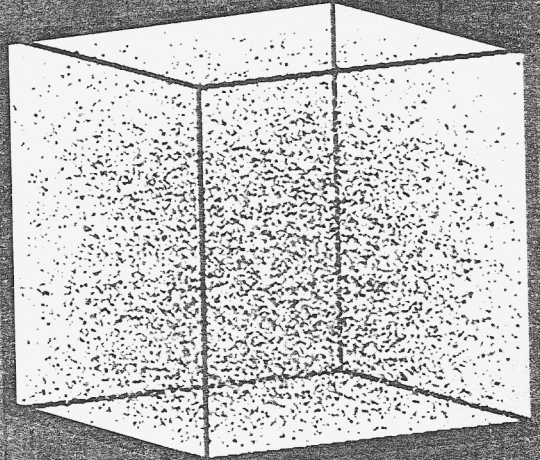
Lawrence Livermore National Laboratory
Technical Information Department's Digital Library
<http://www.llnl.gov/tid/Library.html>



Engineering Technology Reports

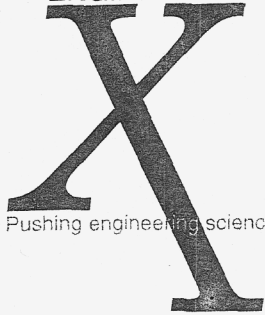


Volume 2: Technology Base



September 2002

ENGINEERING



Pushing engineering science to the Xtreme

Acknowledgments

Scientific Editing
Camille Minichino

Graphic Design
Jeffrey B. Bonivert

Art Production/Layout
Debbie A. Marsh
Irene J. Chan
Lucy C. Dobson
Kathy McCullough

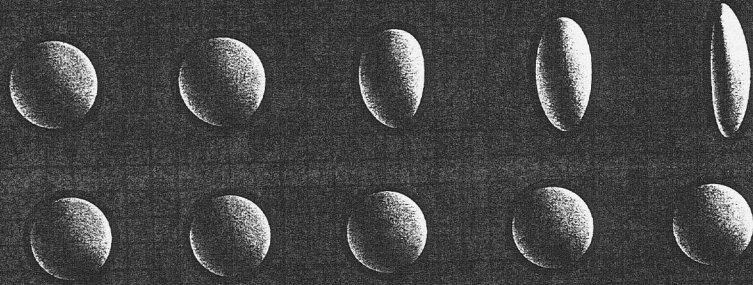
**Document Approval
and Report Services**
Cynthia Tinoco

Cover:

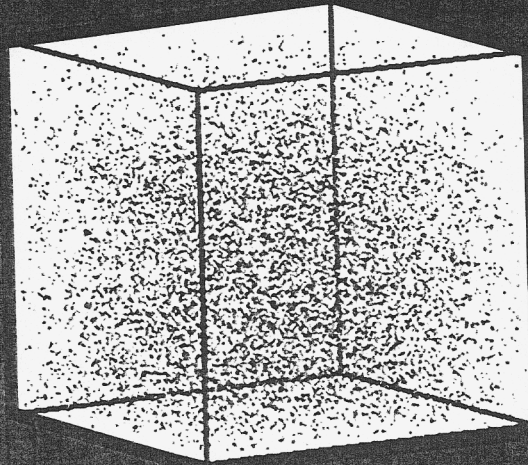
Computational graphics of particle motion and the effects of Weber number on drought deformation.



Engineering Technology Reports



Volume 2:
Technology Base



September 2002

Introduction

Glenn Mara, Associate Director for Engineeringv

Center for Complex Distributed Systems

Strategy and Capability for Communications and Networking

A. J. Poggio3

Characterization of Seismic Propagation and Signal Generation for Vehicle Tracking Systems

D. Harris, D. B. McCallen, D. W. Rock, P. Lewis4

Compensated Optical Communications

C. A. Thompson, L. Flath, R. Hurd, R. Sawvel5

Contact Constitutive Relationships for Interface Surface Features

C. R. Noble6

Extreme Bandwidth Security Tools

B. Bodtker, W. J. Lennon, D. Colon7

High-Resolution Video Surveillance

C. Carrano, J. Brase8

Radar Vision

K. Romero, G. Dallum, J. E. Hernandez, J. Zumstein9

Sensor-Driven Estimation of Chemical, Biological, and Nuclear Agent Dispersal

D. B. Harris10

Ultra-Wideband Communications System on a Chip

C. McConaghy11

Evaluation of Micromachined Inertial Sensors for Distributed Networks

C. Lee, R. R. Leach, Jr., T. Woehrlé12

Wireless Network on Demand

B. Henderer13

Center for Computational Engineering

Development of Multi-Phase Flow Modeling Capability

T. Dunn, L. Daily, R. Couch17

Engineering Visualization Lab

M. Loomis, R. M. Sharpe, K. Mish18

Enhanced Fluid Dynamics Capability and Multidisciplinary Coupling in ALE3D <i>R. McCallen, T. Dunn, G. Laskowski</i>	19
Planning Tool for Site Remediation Simulation <i>J. Stewart, R. Glaser, A. Lamont, A. Sicherman, T. Hinkling</i>	20
Coupled Engineering Simulation Tools: Solids, Fluids, and Chemistry <i>C. Hoover, A. Shapiro, R. Ferencz</i>	21
New Surface Loads and Display Capabilities in DYNA3D <i>J. Lin</i>	22
Advances in Implicit Finite-Element Algorithms in NIKE3D <i>M. A. Puso</i>	23
Development of Computational Capability for MEMS-Based Technologies <i>M. A. Havstad, J. D. Morse</i>	24
Visualization and Data Management Tools: GRIZ4, Mili and XMiliCS <i>D. Speck, E. Pierce, L. Sanford</i>	25
ParaDyn Update: Parallel Interface Algorithms <i>A. De Groot, R. Sherwood, C. Hoover</i>	26
 Center for Microtechnology	
Integrated Microsyringe Arrays for Chip-Scale Fluid Control <i>M. Maghribi, P. Krulevitch</i>	29
Mesoscale NIF and Omega Laser Targets for High-Energy-Density Experimental Science from Nanofabrication <i>R. Mariella, Jr.</i>	30
Microstereolithography for Fabrication of Mesoscale Structures with Microscale Features <i>V. Malba, A. F. Bernhardt, C. D. Harvey, L. Evans</i>	31
Optical Coating Technology <i>D. Sanders, J. Wolfe</i>	32
Optical Pressure Sensor <i>M. D. Pocha, R. R. Miles, G. Meyer, T. C. Bond</i>	33
Process Development for High-Voltage Photovoltaic Arrays <i>G. Cooper, N. Raley, T. Graff</i>	34

Rapid Fabrication of Microfluidic Devices by Replica Molding of Polydimethylsiloxane (PDMS)	
<i>L. R. Brewer, K. Rose, O. Bakajin, P. Krulevitch</i>	35

Remote Hydrogen Sensor	
<i>D. R. Ciarlo</i>	36

Center for Nondestructive Characterization

Distributed Processing Algorithms for Reconstruction and Rendering	
<i>G. P. Roberson, P. C. Schaich, H. E. Jones, M. W. Kartz</i>	39

Enhancements in Infrared NDE Techniques	
<i>W. O. Miller</i>	40

High-Precision Quantitative Tomography of Mesoscale Targets	
<i>W. Nederbragt, S. Lane, D. Schneberk, T. Barbee, J. L. Klingmann, R. Thigpen</i>	41

Linear Array Computed Tomography	
<i>K. Dolan, J. Fugina, J. Haskins, R. Perry, R. D. Rikard</i>	42

Neutron Radiography Beam Stop	
<i>B. Rusnak</i>	43

Rapid High-Resolution Ultrasound Tomography	
<i>J. Kallman, E. Ashby, D. R. Ciarlo, G. Thomas</i>	44

Synchrotron Microtomography at LBNL's Advanced Light Source Facility	
<i>K. Dolan, D. Haupt, J. Kinney, D. Schneberk</i>	45

Three-Dimensional Profilometer	
<i>M. W. Bowers, D. W. Swift, G. W. Johnson</i>	46

Center for Precision Engineering

Engineering Mesoscale Initiative	
<i>D. Meeker, R. Mariella, Jr., H. Louis</i>	49

Fast Tool Servo Application to Single-Point Turning Weapons Physics Targets	
<i>R. C. Montesanti, D. L. Trumper (MIT), J. L. Klingmann</i>	50

Other Technologies

Frame Extraction and Image Processing in Scene Analysis	
<i>A. Gooden, L. Scott</i>	53
Surface and Volumetric Flaw Distribution in Brittle Materials	
<i>R. A. Riddle, C. K. Syn, S. Duffy, J. Palko, E. Baker (Connecticut Reserve Technologies)</i>	54
Nitrogen Augmentation Combustion Systems	
<i>L. E. Fischer, B. Anderson</i>	55
Author Index	
Author Index	59

Introduction

Glenn Mara, Associate Director for Engineering

Engineering has touched on every challenge, every accomplishment, and every endeavor of Lawrence Livermore National Laboratory during its fifty-year history.

In this time of transition to new leadership, Engineering continues to be central to the mission of the Laboratory, returning to the tradition and core values of E. O. Lawrence: science-based engineering—turning scientific concepts into reality.

This volume of Engineering Technical Reports summarizes progress on the projects funded for technology-base efforts. Technology-base projects effect the natural transition to reduction-to-practice of scientific or engineering methods that are well understood and established. They represent discipline-oriented, core competency activities that are multi-programmatic in application, nature, and scope.

Objectives of technology-base funding include:

- the development and enhancement of tools and processes to provide Engineering support capability, such as code maintenance and improved fabrication methods;
- the support of Engineering science and technology infrastructure, such as the installation or integration of a new capability;
- support for technical and administrative leadership through our technology Centers;
- the initial scoping and exploration of selected technology areas with high strategic potential, such as assessment of university, laboratory, and industrial partnerships.

Five Centers focus and guide longer-term investments within Engineering. The Centers attract and retain top staff, develop and maintain critical core technologies, and enable programs. Through their technology-base projects, they oversee the application of known engineering approaches and techniques to scientific and technical problems. The Centers and their leaders are as follows:

- Center for Complex Distributed Systems:
David B. McCallen
- Center for Computational Engineering:
Robert M. Sharpe
- Center for Microtechnology:
Raymond P. Mariella, Jr.
- Center for Nondestructive Characterization:
Harry E. Martz, Jr.
- Center for Precision Engineering:
Keith Carlisle

FY2001 Center highlights

The **Center for Complex Distributed Systems** exploits emerging information technologies to develop unique communications related to data gathering, advanced signal processing, and new methodologies for assimilating measured data with computational models in data-constrained simulations of large systems.

Current Center technology-base activities include: construction of practical wireless communication nodes for application to self-configuring, self-healing networks using commercial off-the-shelf hardware; acquisition and education on usage of commercial wireless communication network simulation tools; deployment of seismic sensors at the proposed Yucca Mountain geologic repository to gather data for application of array processing software in site monitoring; computer code implementation of model update algorithms into an application-ready package for updating and optimization of structural models based on observed data; modification of finite element contact surfaces to include omni-directional behavior necessary for modeling contact surfaces with complex surface details; and construction of wireless vibration sensors for application in NIF ambient vibration monitoring.

These technology-base projects are delivering application-ready tools into the hands of engineers supporting programs, and thus serve a critical link in transitioning from research to practice.

The **Center for Computational Engineering** orchestrates the research, development and deployment of software technologies to aid in many facets of LLNL's engineering mission. Computational engineering has become a ubiquitous component throughout the engineering discipline. Current activities range from tools to designing the next generation of mixed-signal chips (systems on a chip) to full scale analysis of key DOE and DoD systems.

Highlights of the Center's technology-base projects for FY2001 include enhancements of engineering simulation tools and capabilities; progress in visualization and data management tools; and updates in parallel interface algorithms. The Center has offered a real-world computing capability that opens the door to solving a wide variety of fluid/solid interaction problems in transportation, aerospace, and infrastructure settings.

The mission of the **Center for Microtechnology** is to invent, develop, and apply microtechnologies for LLNL programs in global security, global ecology, and bioscience. Its capabilities cover materials, devices,

instruments, or systems that require microfabricated components, including microelectromechanical systems (MEMS), electronics, photonics, microstructures, and microactuators. Center staff have achieved considerable national recognition for the successes demonstrated in Chem-Bio National Security Program instrumentation, supported by the DOE and the Defense Intelligence Agency. The majority of the Center's technology-base projects support defense programs and nonproliferation. These include the application of high-voltage photovoltaics, microaccelerometers, and fabrication techniques to physics experiments that support Stockpile Stewardship.

Highlights in FY2001 include integrated microsyrring arrays for chip-scale fluid control; meso-scale laser targets for high-energy-density experimental science; microstereolithography for microfabrication; and process development for high-voltage photovoltaic arrays.

The **Center for Nondestructive Characterization** advances, develops and applies nondestructive characterization (NDC) measurement technology to significantly impact the manner in which LLNL inspects, and through this, designs and refurbishes systems and components. The Center plays a strategic and vital role in the reduction-to-practice of scientific and engineering NDC technologies, such as acoustic, infrared, microwave, ultrasonic, visible and x-ray imaging, to allow Engineering in the near term to incorporate these technologies into LLNL and DOE programs.

This year's technology-base projects include distributed processing algorithms for reconstruction and rendering, enhancements in infrared techniques, and several advanced applications of computed tomography and neutron radiography.

The **Center for Precision Engineering** is dedicated to the advancement of high-accuracy engineering, metrology and manufacturing. The Center is responsible for developing technologies to manufacture components and assemblies at high precision and low cost; developing material removal, deposition, and measurement processes; and designing and constructing machines that embody these processes.

The scope of work includes precision-engineered systems supporting metrology over the full range of length scale, from atom-based nanotechnology and advanced lithographic technology to large-scale systems, including optical telescopes and high energy laser systems. A new focus is the manufacturing and characterization of "meso-scale devices" for LLNL's NIF. Millimeter-scale physics experiments will provide data about shock physics, equation of state, opacity, and other essential measurements of weapons physics.

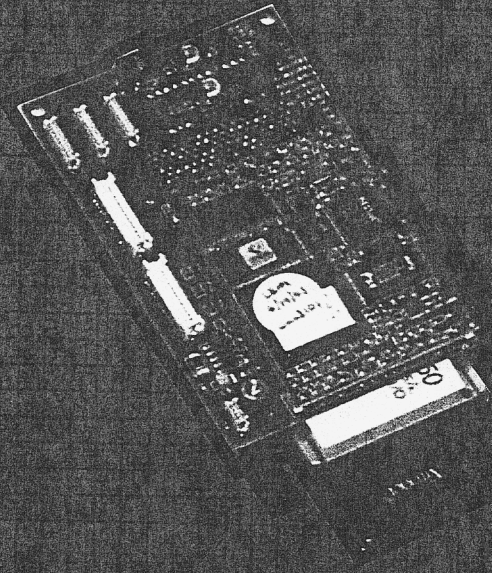
FY2001 highlights include a fast tool servo application to single-point turning weapons physics targets, and surface and volumetric flaw distribution in brittle materials.

Science-based engineering

Our five Centers develop the key technologies that make Laboratory programs successful. They provide the mechanism by which Engineering can help programs attract funding, while pioneering the technologies that will sustain long-term investment.

Our Centers, with staff who are full partners in Laboratory programs, integrate the best of mechanical and electronics engineering, creating a synergy that helps turn the impossible into the doable.

Center for Complex Distributed Systems



Engineering
Engineering
Engineering

CMU

Strategy and Capability for Communications and Networking

A. J. Poggio

The purpose of this technology base project was to bring together the required elements for an Engineering capability in communications and networking (C&N) so that the Directorate could better serve its customers in the programs and in the Work-for-Others regime.

Spiros Dimolitsas, former Associate Director for Engineering, envisioned a scenario where the activities being executed by engineers in C&N would be organized, enhanced, and collocated when possible. Included in this vision was the development of C&N to the level of an Engineering core technology.

To efficiently establish a roadmap for a C&N capability, we chose to create a catalog of LLNL strengths and weaknesses in this arena. It was defined to encompass RF, optics, photonics, networks, and security. Communications theory, analysis, and modeling were critically assessed in terms of capability level; need, in the context of present and anticipated projects at LLNL; and potential customers in the programs and elsewhere. Such a view lent itself to the definition of requirements in the technology base.

Similar assessments were carried out in the areas of communications systems and testing. It was apparent that LLNL's core strength in remote sensing called for an accompanying strength in C&N, and that capabilities in networks, wideband and optical communications, and systems integration warranted further attention and advancement.

The development of a capability requires access to state-of-the-art equipment for executing tasks and performing R&D. To this end, we sought to create a strategic plan for equipment purchase that would be complementary to purchases that had been made in FY01 using IGPE funds.

We also demonstrated the universality of the C&N capability that was being organized by assimilating equipment from the programs that would be able to service LLNL at large. In addition, plans were finalized for the establishment of a National Transparent Optical Network (NTON) lab and for an unclassified communications lab in what was then referred to as the C&N Laboratory.

During FY01, a classified communications laboratory was established within the confines of the Electromagnetics Laboratory. A small library was pulled together to support the capability represented by the laboratories. To round out the beginning stages of this capability, we scoped out the needs of a communications design "workstation," and we coordinated the acquisition of a high-end computer and communications design software using alternative sources of funding.

It was apparent that a core technology in C&N would require the establishment of relationships with prominent practitioners across the nation. We felt that relationships with universities would provide fruitful sources for technology and expertise as well as recruiting opportunities for students. Several exchange visits were made during FY01 with the University of Maryland; holder of an extraordinarily strong reputation in C&N. They visited LLNL and briefed us on their interests and ongoing projects and, in return, we briefed their staff members on the same issues.

Strong interactions also took place with key staff members at the University of Texas, Dallas, and the Virginia Polytechnic University. To ensure the relevancy of the capability that we were developing, we also interacted with several government agencies that were very active in the C&N arena. Meetings were held with the elements of the Joint Chiefs of Staff, the Laboratory for Telecommunication Science (UM and NSA), CIA, NSA (IOTC), the Navy Information Warfare Agency, the Army's CECOM, and the SPAWAR Network Modeling and Simulation Branch. Throughout, we received encouragement regarding our development strategy, and a desire to keep a close working relationship. Included in these interactions were also many exchanges of lessons learned.

At the end of FY01 we had developed a strategy for a strong C&N capability; prepared and equipped a communications laboratory in a classified area; laid plans and coordinated the advanced stages of preparing an unclassified C&N laboratory; assembled a C&N design workstation with software; and had initiated and nurtured relationships that would help us grow this capability.

Characterization of Seismic Propagation and Signal Generation for Vehicle Tracking Systems

D. Harris, D. B. McCallen, D. W. Rock, P. Lewis

Remote detection, tracking, and identification of vehicles are important in battlefield and surveillance applications. Networks of seismic arrays may be deployed to perform these functions. How well these systems will perform is critically dependent on how well vehicles couple vibration energy to the ground and how efficiently the generated seismic energy propagates to the sensor arrays. To determine these characteristics we carried out two experiments at the Yucca dry lakebed at the Nevada Test Site (NTS).

In the first of our experiments we used a log-linear array of eight seismic instruments to determine the attenuation rate of seismic wave propagation. From this deployment, we learned that seismic signals propagate primarily as surface waves and that the attenuation rate is large at high frequencies.

The second experiment consisted of 20 instruments deployed in a fan-shaped array to characterize the seismic radiation pattern of tracked and wheeled vehicles. We learned that tracked vehicles project seismic energy predominantly in the direction of motion, and that this effect becomes more pronounced as frequency increases.

Seismic sensors may be a component of an instrumented battlefield along with radars, acoustic sensors and optical systems. One of the principal issues is how

to increase the "standoff" (detection range) of systems so that relatively large areas can be observed with a modest deployment of sensors.

Our deployments demonstrated several key features of signal generation and propagation that may guide the engineering of new seismic sensors and contribute to processing algorithms.

Usable signals are observed at all ranges, but are restricted to relatively low frequencies (much less than 10 Hz) at the greater ranges (2000 to 4000 m). This observation, corroborated by experience with seismic arrays in Norway observing rail traffic, suggests that new ground instrumentation development for long-range vehicle tracking should focus on low-frequency performance.

Perhaps the most interesting and new discovery came from work with our vehicle seismic characterization testbed, shown in Figure 1. We determined that tracked vehicles exhibit a pronounced seismic wave radiation pattern. At low frequencies, seismic energy is projected predominantly fore and aft in the line of travel (Figure 2). At higher frequencies, it is even more directional, being projected primarily forward in the direction of travel.

This observation impacts estimates of vehicle detectability and sets a criterion to be met for realistic simulation of seismic signals generated by moving vehicles.

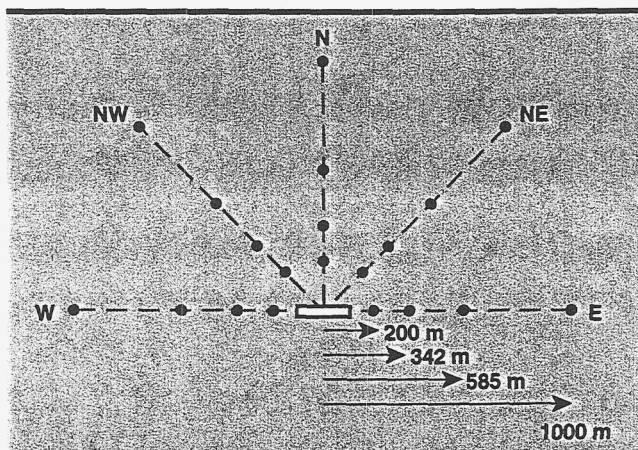


Figure 1. Fan-shaped vehicle characterization array.

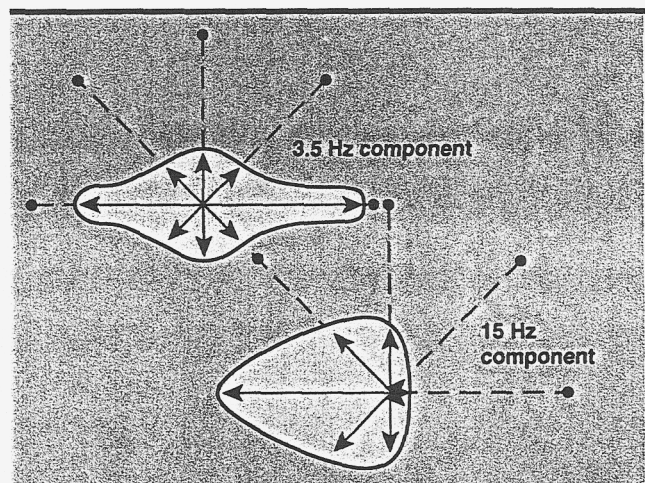


Figure 2. Seismic wave radiation patterns at two frequencies for a tracked vehicle.

Compensated Optical Communications

C. A. Thompson, L. Flath, R. Hurd, R. Sawvel

High-bandwidth, secure/covert communications is an important piece of sensor-based systems for DOE, DoD, and intelligence community applications. Free-space optical systems provide high-bandwidth, covert, wireless communications, but are limited by atmospheric turbulence. We have proposed an Adaptive Optics (AO) test-bed system that allows flexible testing of new concepts and technology for optical communications applications. This new capability will lead to future projects from current LLNL sponsors in national security and defense, and put LLNL in a position to make significant contributions to the field of free-space optical communications.

Wavefront compensation for free-space systems will improve performance by reducing power requirements, increasing data bandwidths, and lengthening transmission distances. Leveraging the improvements in MEMS technology makes wavefront compensation feasible.

The goals for FY01 were to complete and demonstrate an integrated optical communications and wavefront control test-bed based on MEMS technology, using equipment purchased with Engineering capital equipment funding in FY00. As shown in Figure 1, we have designed and assembled the wavefront control system. We have not yet demonstrated closed loop performance, due to safety concerns with potential electrical hazards.

The electronics package shipped with the MEMS device is a prototype unit. After investigating how the high-voltage electronics box (Figure 2) was put together, we identified and rectified five potential electrical safety issues. We also collocated all electronics in one enclosure (Figure 3), which made sense to us from both safety and practical standpoints. The new system has been inspected and approved by an AHJ (Authority

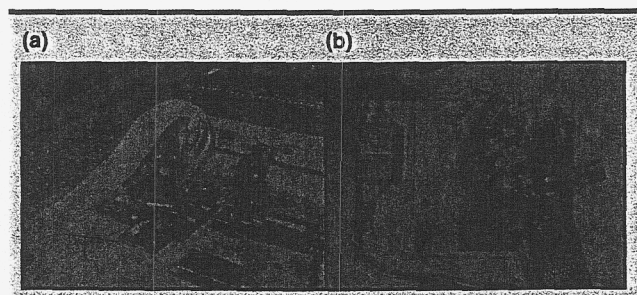


Figure 1. (a) MEMS mirror integrated into the Adaptive Optics Test-bed and (b) Adaptive Optics "Lunchbox." MEMS technology allows miniaturization of the system.

Having Jurisdiction) as per Document 16.3 of the LLNL Environment, Safety and Health Manual.

A Boston Mircomachines 140 actuator MEMS mirror has been successfully integrated into our AO test-bed (Figure 1a). The MEMS device has been used recently as an aberrator in the AO test-bed. A second wavefront control device (in this case a liquid crystal spatial light modulator (SLM)) is used to correct the aberrations caused by the MEMS device. In the near future, the MEMS device will actually be used as the corrector element for an aberration placed into the system (most likely by the SLM).

The addition of the MEMS device to the AO test-bed has allowed for improvements in wavefront control algorithms and software. We have also built a smaller AO system as a proof of principle (Figure 1b). Because of its small size (approximately 40 cm x 30 cm) we have dubbed it the "AO Lunchbox." Currently the system runs with electronics shown in Figure 3 and a desktop PC. We have not yet run the AO system in this package. Closing the loop and modifying the system will be a future project.

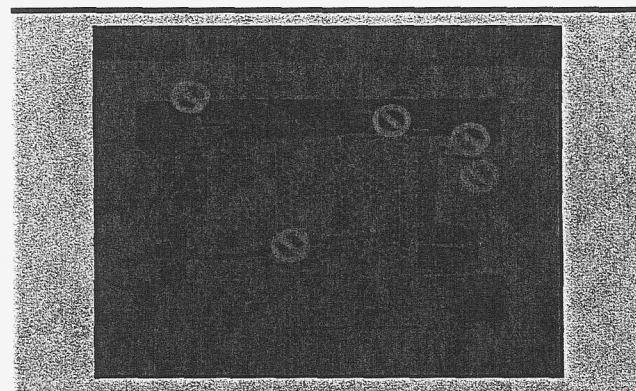


Figure 2. High-voltage electronics box for MEMS system. The red symbols indicate potential hazards we identified and rectified.

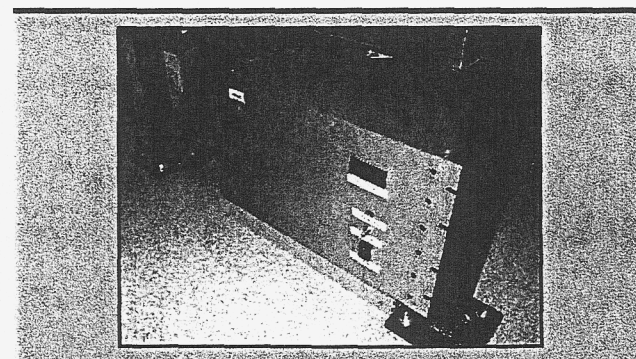


Figure 3. New completed electronics enclosure.

Contact Constitutive Relationships for Interface Surface Features

C. R. Noble

The contact algorithms at our disposal currently do not have the capability to accurately model the local topology of a structure's contact interface, where load is often transferred between components through the use of geometrical discontinuities. The presence of discontinuities is a common feature in many mechanical systems, such as Hard and Deeply Buried Targets (HDBT) and large multi-bodied structures such as concrete dams and bridges. Our objectives are: 1) determine a constitutive law that accounts for interface surface features; 2) validate the algorithm with experimental data; 3) implement the algorithm into FEM codes; 4) develop university collaborations; and 5) enhance our relationship with sponsors, the US Bureau of Reclamation (USBR).

Hardened Deeply Buried Targets consist of concrete tunnels surrounded by large rocks buried deep within a soil mass. To accurately simulate the response of these structures, the rock joints need to account for damage or degradation along the interface, as well as dilatancy (volume increase under simple shearing stress) and local topology effects. It is not realistic to assume that a rock joint can be modeled with a smooth, flat interface.

To model rock interfaces, a more detailed traction-displacement law is required. Similarly, concrete dam structures may consist of 30 or more contact interfaces that include shear keys (see Figure 1). These shear keys result in unique directionality effects along the concrete interfaces similar to that of rock interfaces.

Our accomplishments to date have included an extensive literature review on the existing contact algorithms, as well as identifying the contact algorithm capabilities needed for future work on large multi-bodied structures (HDBT and concrete dams).

The first capability needed is the ability to define separate slide surfaces along user-defined planes. The reason for these planes is best described by looking at the finite element model of Morrow Point Dam, a concrete arch dam, in Figure 2. Because of the shear keys located on each contraction joint, the separate concrete blocks are free to move only vertically along these planes and normal to the adjacent block.

Once directionality has been added to the contact surface, it will be useful to have separate cohesive/shear strength terms (C_1/τ_1 , C_2/τ_2) for the upstream/downstream direction and the vertical direction. Finally, it is imperative that the contact surface be able to provide shear resistance as a function of the gap

distance. The reason for this is that the shear keys provide shear resistance up until the normal gap between the blocks opens more than the thickness of the shear keys (Figure 1).

In addition to identifying the needed capabilities, the USBR is beginning to perform shake table tests on typical concrete lifts used in dam structures. This data will be used to validate the new contact algorithm. Funding (\$80 K) was also recently secured from the USBR to perform a seismic evaluation of Morrow Point Dam. One of the primary project objectives is to incorporate the contact features already discussed and run a suite of suitable test problems.

Other accomplishments include consulting with UC Berkeley and obtaining work on subterranean effects (HDBT) for LLNL's DNT/Q Division to validate and import finite element tools, such as contact algorithms, for use in analyzing underground facilities.

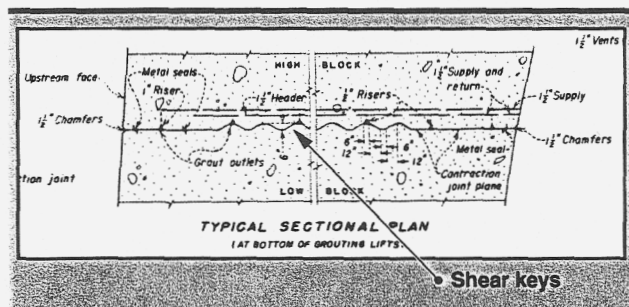


Figure 1. Shear keys common to concrete arch dams.

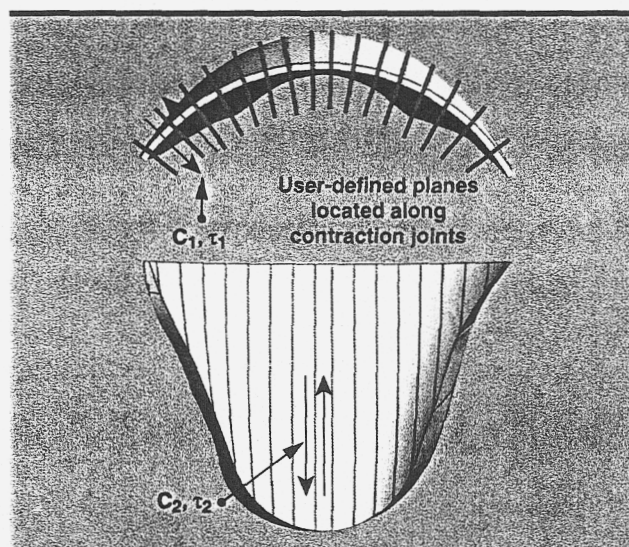


Figure 2. Needed contact algorithm capabilities.

Extreme Bandwidth Security Tools

B. Bodtker, W. J. Lennon, D. Colon

While intrusion detection and firewall protection are available at multi-Mb/s data rates, cost-effective analysis and management of multi-Gb/s data streams are currently beyond the state of the art. Organizations like LLNL will be depending on very-high-speed networks for a variety of collaborations in the near future, but can no longer deploy networks for regular business without being able to manage their security. We are leveraging our role in high-bandwidth networking to strengthen our collaboration between nationally recognized experts in different aspects of high performance network analysis and security management. The goal is to jump-start the commercial development of security tools so that they are readily available when LLNL and other organizations require multi-Gb/s networks for normal production activities.

As a first example of a necessary security tool, we believe it is feasible to create a network intrusion detector (NID) that operates at OC-48. Doing experiments and demonstrations at OC-12 will prove feasibility and establish credibility to pursue a larger effort for upgrading the design to the higher rate. The Laboratory has expertise in NIDs, having developed the software currently used at DOE sites for detecting intrusions; this software continues to be developed under the auspices of the Nonproliferation, Arms Control, and International Security (NAI) Directorate.

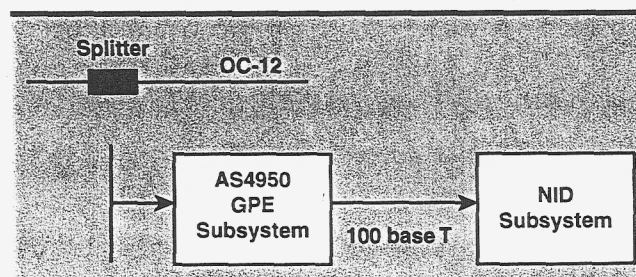
The current capability of the software is sufficient to perform its function on the existing 100 Mb/s networks at these sites, but scaling the performance to high-bandwidth networks is not as simple as running on faster processors. Some hardware assistance is necessary.

Network protocol analyzers on the market are capable of viewing all packets on a network at speeds up to 10 Gb/s, which is a key requirement for intrusion detection. Some of these devices use field programmable gate arrays (FPGA) that could be reprogrammed to perform the pattern matching needed for this function. We felt that collaboration

between a vendor of a programmable analyzer and NID software developers could produce a prototype of a high-bandwidth intrusion detector.

In FY00, we acquired Boeing's FPGA-based AS4950 network protocol analyzer, and began collaborating with Boeing to combine their hardware with NID software to produce an intrusion detector operating at OC-12 (see figure). Boeing was to modify the firmware and software in the AS4950's Generic Processing Engine (GPE) that would support sophisticated pattern matching and filtering functions. This would allow for dramatic reductions in NID-processed packets to levels within the NID's capability. The collaboration has produced a design specification for the Boeing modifications that is currently proprietary to Boeing.

In FY01 we developed both the application program interface (API) and controller interface (CI) software packages necessary to interact with the NID software. The CI is GUI-based and user-friendly. We opted to use the SNORT NID package as it was both well understood and in the public domain and, as such, allowed us access to the source code for any modifications we required. We successfully integrated the three software elements in a UNIX-based PC and were awaiting completion of Boeing's development effort at fiscal year's end. If FY02 funding is secured we will integrate LLNL's software with Boeing's hardware and begin testing with artificially generated traffic. From this we hope to leverage what we learned to extend the technology to an OC-48 rate.



The OC-12 system block diagram.

High-Resolution Video Surveillance

C. Carrano, J. Brase

Atmospheric and optical aberrations reduce the resolution and contrast in surveillance images recorded over long (>1 km) horizontal or slant paths. A capability of improving such images is of great interest to the DoD/intelligence communities. In this project, we proposed to demonstrate a prototype remote surveillance system that corrects these aberrations and improves resolution in such scenes using speckle imaging techniques.

Speckle imaging techniques require multiple frame acquisition of short exposure imagery to recover the high-resolution information that is lost in a typical blurred long-exposure image. During FY01, we delivered a prototype remote video surveillance system consisting of the following:

Hardware:

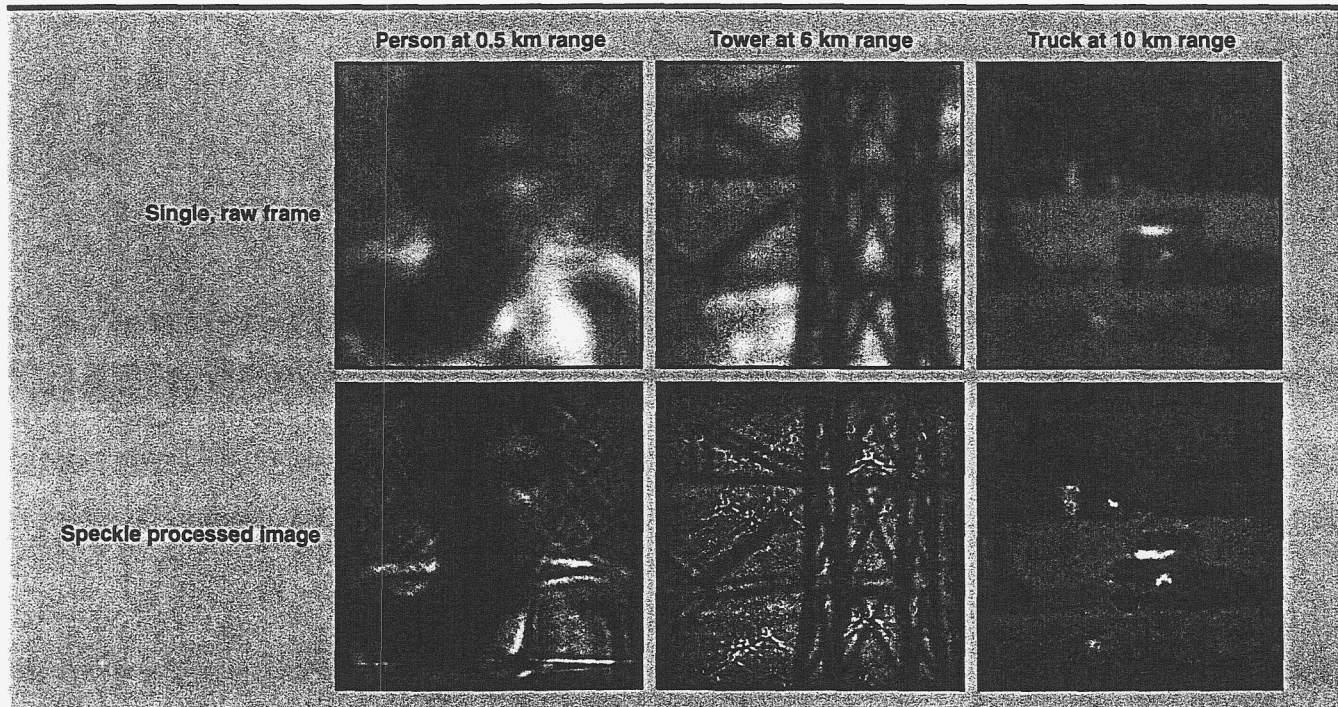
- Celestron 8-in. telescope and associated optics
- Qimaging Retiga 1300 CCD camera—1280 × 1024 pixels, 12-bit camera capable of short exposures down to 35 μs
- Gateway laptop with Firewire connection for the data transfer

Software:

- Data acquisition software (Empix Imaging Northern Elite)
- Data preprocessing algorithms in IDL
- Speckle reconstruction software

We performed several horizontal-path imaging experiments from building roof tops this year with a variety of targets including resolution targets, people, vehicles and structures. We obtained excellent results with the speckle processing: with a sub-resolution point target, speckle processing resulted in a spot with 1.3 times the telescope diffraction limit. We also demonstrated improved resolution in both near- and far-range scenes of interest. Example results are shown in the figures.

To make this capability more attractive to potential customers, we plan to perform more experiments and analysis, directed at better quantifying system performance in varying conditions and system parameter configurations, including ranges beyond 10 km. We also plan to use enhanced imagery of personnel and vehicles to evaluate the accuracy of gross biometric and vehicular feature measurement.



Radar Vision

K. Romero, G. Dallum, J. E. Hernandez, J. Zumstein

Special Forces, DARPA, DOE, and the intelligence community have a need for the capability to "see" through walls and smoke. Law enforcement first responders, such as SWAT teams, require a portable, affordable device that will provide them real-time, full-motion images of a crime scene through exterior and interior building walls, and through smoke. The ability to differentiate between perpetrators and victims, and to locate weapons, is highly desired. To get a good quality image useful for shape recognition, an ultra-wideband scanning radar system or an array of radars, with suitable imaging algorithms, is needed to obtain a high resolution Synthetic Aperture Radar (SAR) image of the scene (Figure 1).

LNL is a world leader in developing high-resolution SAR imaging systems for NDE applications such as the inspection of bridge decks. We have pioneered the use of low-power ultra-wideband impulse radar scanning systems and arrays for high-resolution imaging of materials.

The plan for the first year was to develop a test-bed for scanning a single radar in a 2-D vertical plane under computer control to simulate different array configurations and electronic beam steering. This test-bed consisted of various elements, which included the timing circuits (Figure 2a) and software for controlling the firing of the radars; the radars themselves (Figure 2b); and finally the data acquisition software.

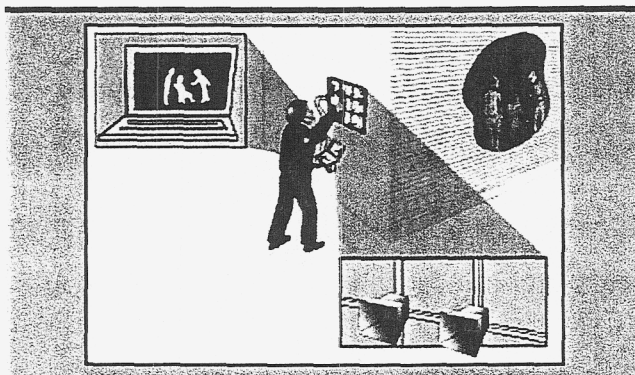


Figure 1. Low-power ultra-wideband impulse radar scanning system.

The test-bed has allowed us to acquire SAR data of a variety of objects for testing and evaluating different imaging concepts. We created a theoretical model for the system response of scanning the vertical plane along the target. Then we varied both the lateral and longitudinal placement of the target and acquired real data. By comparing the real data to simulated data, we were able to verify the functionality of the system. By testing different scanning patterns and radar antenna placement, we were able to get additional insight into optimal radar placement and scanning algorithms.

During the second year, different imaging algorithms and an expanded number of radar elements (transmitters, receivers) will be tested to determine the best approach for developing a portable SAR imaging system for imaging objects from a distance through air and a variety of wall materials.

Our FY01 results and expected FY02 efforts will provide the groundwork for attracting follow-up funding for a complete portable imaging system prototype for intelligence applications.

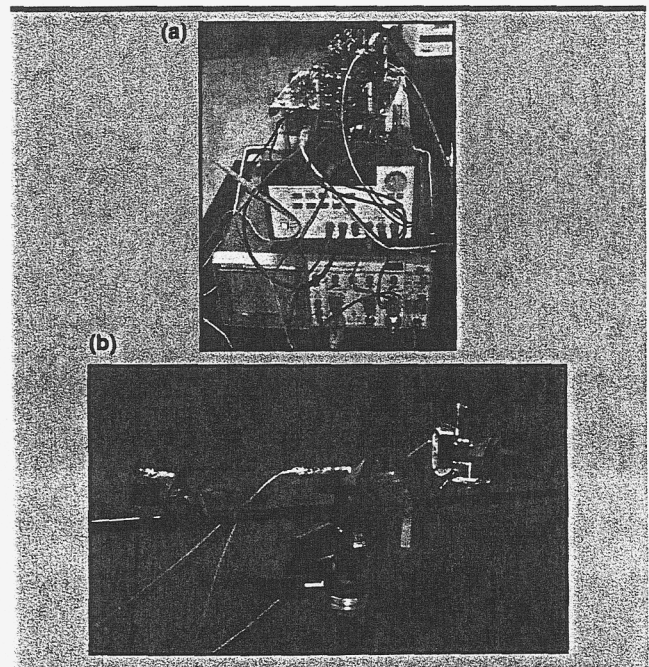


Figure 2. (a) Timing circuits and (b) radars for test-bed.

Sensor-Driven Estimation of Chemical, Biological, and Nuclear Agent Dispersal

D. B. Harris

This proposal was developed jointly with the Energy and Environment Directorate, NAI, and Computations at LLNL. The proposal identified a new research/business opportunity for NARAC and Engineering, entailing a shift in NARAC's current operations from open-loop projection of future plume distributions to closed-loop estimation of past, present, and future plume distributions. The proposed system is an instance of a more general paradigm emerging in the physical sciences: complex numerical models for physical processes developed originally to explain experimental observations statically are embedded in real-time, sensor-driven systems that dynamically estimate parameters of interest. This paradigm represents the maturing of scientific models into operational systems.

Sensor-driven estimation of dispersing plumes would position LLNL to compete vigorously for significant new research and operational opportunities in a variety of environmental, civilian, and military atmospheric release advisory applications. These applications involve the detection and tracking of radiological, chemical, and biological agents/pollutants released into the atmosphere.

NARAC currently has sophisticated dispersion models for predicting patterns of mean plume concentration, given a source, but no systematic capability to invert for source locations and characteristics, given plume observations.

We proposed to develop an inversion capability by establishing the modeling, estimation, and communication framework to exploit data, first from networks of pre-deployed sensors at cooperating sites, then from next-generation networks of rapidly-deployed, mobile sensors. The latter can be deployed after detection, and reconfigured as a release incident unfolds. The significance of networks of mobile sensors is that the condition of ill-conditioned inverse problems may be improved by judicious placement of sensors to acquire, surround, and track an evolving plume.

We envisioned a project-deploy-correct cycle, in which NARAC forecasts guide sensor placement in real time, and network data is fed back to update the models. The cycle may repeat from initial detection until final plume dilution.

The main applications of interest were identified as treatment and protection of civilian and military populations in scenarios of chemical, biological, and radiological attack; accidental industrial release of toxic materials; accidental release of radionuclides from cooperating DOE and DoD facilities; and bomb damage assessment and minimization of collateral civilian exposure in strikes against WMD facilities.

New technical capabilities must be developed, acquired, or adapted to support application of basic atmospheric dispersion science to practical inverse problems; adaptation of robust military communication technologies to ensure that field data can be communicated to NARAC under rapid-deployment conditions; and integration of miniaturized, fast-response biological and chemical agent sensors under separate development into an operational forecast and inversion system.

The expected result of the proposed initiative was a set of field-validated technologies that would radically expand NARAC's operational capabilities: codes to estimate rapidly source location and characteristics from real-time concentration observations; codes to estimate past plume concentration and dosage in space and time; codes to forecast plume concentration and dosage in an ensemble of wind fields; and a communication framework for integrating these models with current and next-generation theater meteorological and concentration sensors.

The technologies to be developed under this initiative have natural marketing outlets through existing LLNL programs. Several NAI programs have interests in plume tracking and agent source estimation problems. Military applications include planning for strikes against WMD facilities to minimize collateral civilian exposure and to perform bomb damage assessment.

The same techniques have domestic civilian applications of interest to NAI: assessing and possibly mitigating the impact of terrorist attacks on civilian targets during special events. In principle, the same services could be offered to the wider base of 120 municipalities specified under the Nunn-Lugar-Domenici (NLD) amendment of 1997, for assistance in incidents of domestic terrorism. The rapid assessment and initial detection teams designated under NLD could be the field operational arm of an advisory system promoted by NAI and involving NARAC.

Ultra-Wideband Communications System on a Chip

C. McConaghy

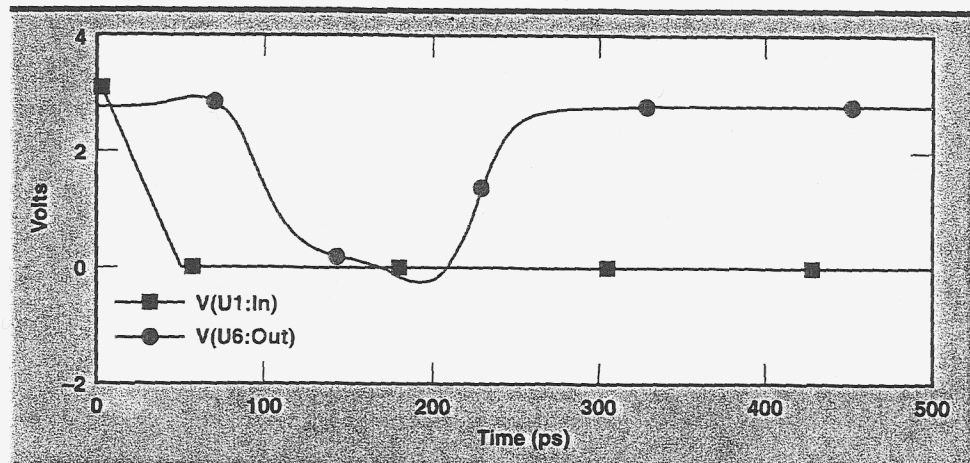
Ultra-Wideband (UWB) communications systems transmit data with pulses as short as 100 ps. These pulses have very low probability of detection and can be used in very-low-power communication systems. UWB communications systems developed previously at LLNL use discrete electronic and microwave components assembled in a hybrid breadboard configuration. The objective of this work has been to incorporate some of the previous work into an application-specific integrated circuit (ASIC).

This work included a survey of available processes, circuit topologies, and computer simulations of the circuits with SPICE. Current resources did not permit circuit layout and fabrication. The most suitable processes available for this work include sub- μm

CMOS as well as SiGe. For example, foundry CMOS with gate lengths of 0.35 to 0.16 μm have gate propagation delays ranging from 61 to 28 ps, which is more than adequate for generating the UWB pulse.

Modeling was done of a pulse generator capable of generating a pulse with 100 ps width. Additional modeling was done on an amplifier that could amplify these pulses such that they could drive the 50- Ω load of the antenna. Circuits were also modeled for encoding data with these pulses. The actual modeling was done using real transistor models from the foundry that would do the later circuit fabrication.

The modeling results (see figure) indicated that, indeed, short (100 ps) pulses could be generated in 0.35 CMOS, data encoded, and amplified to the 50- Ω level.



Simulation results of the UWB pulse generator in 0.35- μm CMOS. The blue trace is the step input to the generator; the red trace is the 100-ps pulse output.

Evaluation of Micromachined Inertial Sensors for Distributed Networks

C. Lee, R. R. Leach, Jr., T. Woehrle

Distributed wireless sensor networks made up of hundreds to thousands of individual sensor nodes can be deployed in locations or on structures in severe, inaccessible, remote environments. These networks can be used to collect information; monitor the state/health of a structure or mechanical system; or validate large-scale computational simulation models. This project has developed a test capability for evaluating accelerometer sensor packages for implementation in distributed networks.

Two requirements for accelerometer sensors in distributed networks are 1) that the overall package be as small as possible, and 2) that the sensors be sensitive enough to measure motion in a near DC-level frequency range. Capacitive-type micromachined accelerometers can meet these requirements, due to their miniature size and frequency bandwidth. However, accelerometers with small inertial proof masses may have trouble differentiating signals from background noise at low excitation levels and frequencies.

The primary component of the test-bed is an air-bearing horizontal shaker table (Figure 1). The peak-to-peak stroke of the shaker is 6.25 in. Its performance envelope is approximately 0.2 Hz to 200 Hz and 0.01 g to 1.5 g (for single sine frequencies). Input to the shaker table is by a controller that can specify random, single/swept sine, or user-defined time series inputs. Various control or reference accelerometers were used depending on the desired input signal frequency and amplitude range.

A series of off-the-shelf commercial, micromachined (or MEMS) type capacitive accelerometers

were evaluated and their performance was recorded to form a data "library."

Performance of the capacitive sensors with respect to the reference accelerometers was based, initially, upon five classes of input signals: random, burst random, single frequency sine, swept sine, and burst sine. The frequency bandwidth was approximately 0.1 Hz to 200 Hz with various frequency amplitudes. It was determined that three types of input, random, single frequency sine, and swept sine, were sufficient to evaluate the accelerometers.

Results for accelerometer performance are summarized by the (complex) transfer function and by the coherence between the response of the accelerometer under test with respect to the reference accelerometer. These values are presented as a 3-D plot with excitation frequency and excitation amplitude as two abscissa axes. This generates a "surface of sensitivity" that characterizes the accelerometer. For clarity of presentation, these surfaces can be presented as color intensity images. Regions of "good" or "bad" performance can easily be picked out over the range of input excitation frequency and amplitude. Figure 2 shows an image of the real part of the transfer function for the Kistler 8304B2 accelerometer. The data and images of the accelerometers are stored as MATLAB files, allowing easy access and portability.

Note that this evaluation procedure can be applied to any type of accelerometer over any frequency bandwidth and amplitude, provided the vibration shaker equipment can deliver the appropriate excitation. Accelerometer performance can also be evaluated with respect to actual pre-recorded field measurements using the vibration controller's playback capability.

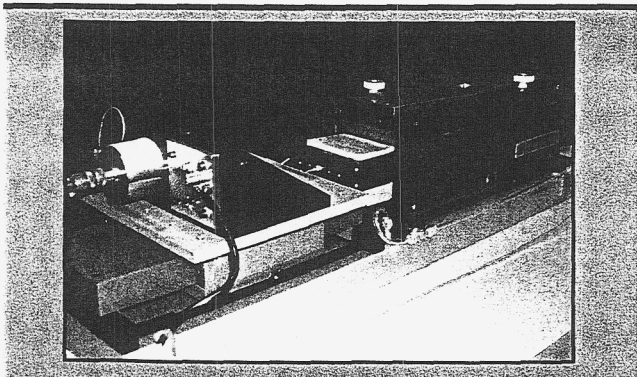


Figure 1. Air-bearing shaker table in test-bed.

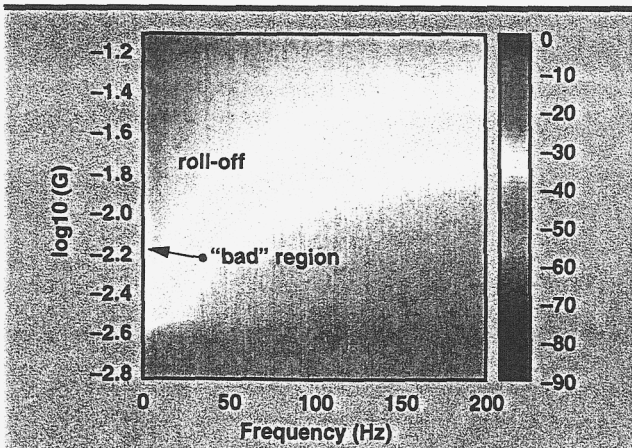


Figure 2. Performance image for test accelerometer (real part of the transfer function).

Wireless Network on Demand

B. Henderer

The goal of this technology base work was to construct a wireless, low-power communications network that would maintain itself. The network would configure itself with the nodes available, add new nodes as they arrived, and reroute paths to handle lost nodes. All of this was to be accomplished with no user intervention. A three-node network was to demonstrate the basics of the design for future work. Commercial, off-the-shelf equipment was to be used to reduce costs.

The Wireless Network on Demand (WNOD) technology base project accomplished all the goals stated above, plus extra features to further test the capabilities of the system (see figures). We purchased several embedded 486 computers and installed Linux on them. We also purchased 802.11b wireless Ethernet cards in PC card format and configured them to operate with the Linux environment on the embedded controller.

Software was developed that accomplished the self-configuring and self-healing aspects of the system. All the nodes have the networking software installed on them. The software was also loaded onto laptop computers running Linux to demonstrate larger network capabilities. This software has successfully operated in five demonstrations and one field deployment.

During pre-testing and the field deployment, range testing was conducted to determine feasibility of the

system. Any distance less than two miles will result in no loss of data. Power consumption is 1.25 W, and the system can run off a hand-sized battery for 1.5 days.

In addition to accomplishing the goals of the technology base work, we demonstrated the ability of the communications node to control sensors. An analog-to-digital converter PC card was installed in the communications node. During the field test, the node gathered data from a ground sensor and reported it back to a base station for display.

Future enhancements of the system would solidify the units as ready-to-use, with limited start-up requirements. A two-PC cardholder PCB is being built and needs thorough testing. This allows the node to operate the wireless network and have space for sensor controls or extra memory. Testing with a larger network (10+ nodes) would help understand engineering requirements for bandwidth usage and network stability. Adding more power-conserving technology to lower the power consumption to less than 1 W is also desirable.

Many projects have shown interest in the WNOD technology. The Cooperative UAV Networks will be using the communications nodes as the primary means of data communications; the Ground Sensing Arrays project can use them to gather data in real time to allow faster analysis; Integrated Optic Capillary Electrophoresis (IOCE) plans to use them to operate equipment remotely; and Lasers Engineering Division has shown interest in the project as a diagnostics tool.

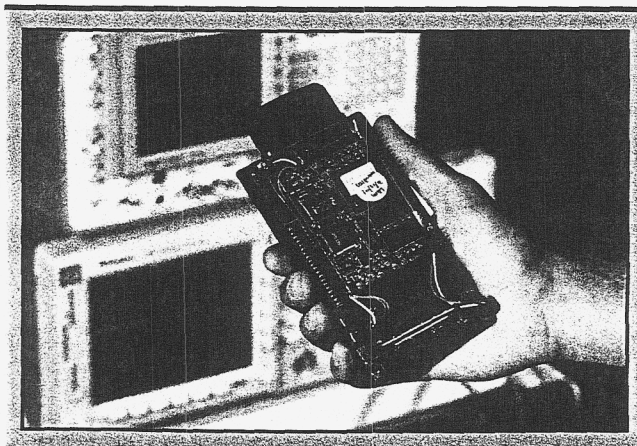


Figure 1. Wireless network node with 486 computer, wireless Ethernet, 10 Mb on-board flash memory for user applications. It is capable of creating a self-configuring, self-healing wireless network.

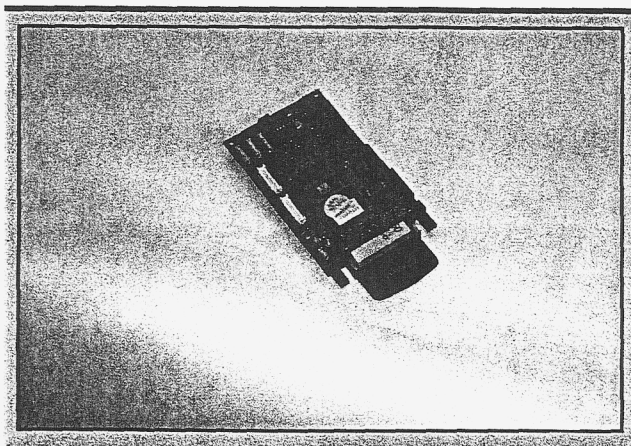
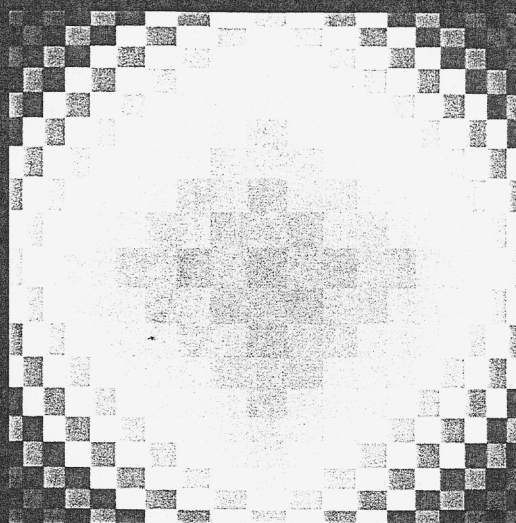


Figure 2. Wireless network node with added 16-channel A/D converter loaded into a second PCMCIA card slot. The second card slot adds versatility.

Center for Computational Engineering



Center for Computational Engineering

CMU

Development of Multi-Phase Flow Modeling Capability

T. Dunn, L. Daily, R. Couch

The motion of fluids plays a significant role in our physical world. Three states (liquid, gas, and plasma) of the four states of matter are classified as a fluid. Even solids behave as a fluid in many situations. Therefore, it is not surprising that the physics describing fluid behavior plays a critical role in the analysis of many realistic engineering problems. The purpose of this project was to enhance LLNL's fluid dynamics capability in the area of multi-phase flow.

Although most flows can be approximated as a single homogeneous fluid, many problems of interest to industry and government agencies are dominated by more complex phenomena. Some complex flows may contain multiple components; reside in multiple phases; involve chemical reactions; or be a combination of all of the above.

Our code development activities built upon the current tools available in the ALE3D multi-physics hydrocode. During the first year of this project, the primary focus has been on discrete particulate transport and free-surface flows.

The particle-tracking module simulates problems involving particulate transport within a carrier fluid. Dilute particle flow is assumed where local aerodynamic forces control the particle's motion. Momentum is transferred from the particle to the fluid through the fluid's continuum equations. Each particle is individually tracked in a Lagrangian reference frame using an equation of motion derived from Newton's second law. The

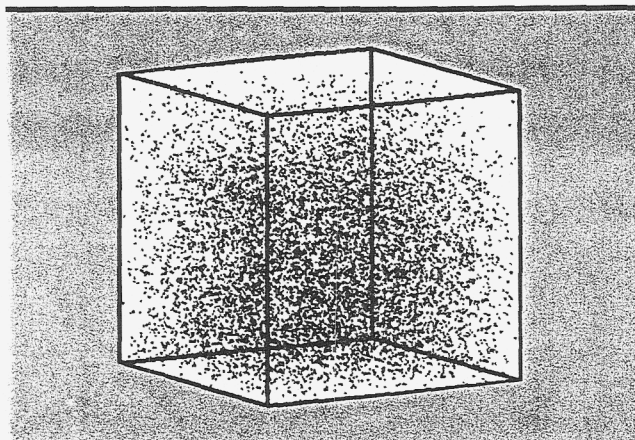


Figure 1. Computation of particle motion in an enclosed box with wall interaction. The particles bounce off the walls until all the momentum is dissipated.

equation accounts for the steady-state aerodynamic and gravity/buoyancy forces acting on the particle. The trajectories are computed with a generic algorithm, so more specific physics may be easily added to the model through additional terms to the equation of motion. The parallel methodology of ALE3D provides fast computations for large problems with many particles.

Bounce models have been added to account for particle-wall interaction. A hard-sphere model is used for the mechanical behavior associated with the collision. The interaction depends on the inertia of the particle. Kinetic energy loss due to friction and inelasticity are accounted for. Figure 1 shows a snapshot of a validation case where a large number of particles are released in a walled container.

Droplet dynamics has been the main thrust of the free-surface modeling effort. The deformation and breakup of droplets involves complex coupling between aerodynamic forces and the droplet response. The Arbitrary-Lagrangian-Eulerian (ALE) formulation in ALE3D is ideally suited to capture the droplet motion. A surface-tension model was added to ALE3D to simulate the intermolecular forces within the droplet. The model is based on minimizing the element energy around the surface of the droplet. In addition, a mesh-relaxation scheme was added to ALE3D, such that the computational grid surrounding the droplet is mapped to the droplet motion, and a constant level of grid refinement near the surface is obtained throughout the simulation.

Figure 2 shows the effects of surface tension on liquid droplets traveling through a gas. Note that the droplet with a small surface-tension coefficient ($We = 3.5 \times 10^8$) exhibits much more deformation than the droplet with a large surface-tension coefficient ($We = 3.5 \times 10^2$).

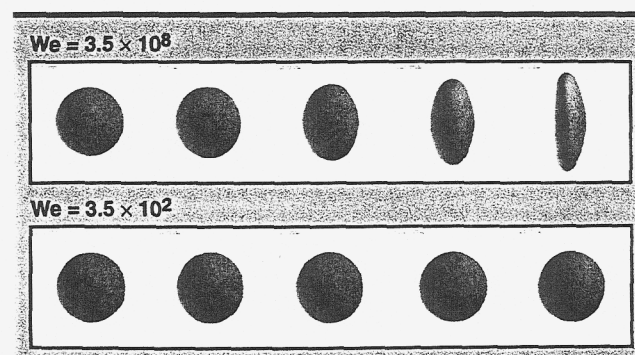


Figure 2. The effects of Weber number on droplet deformation (Weber number is inversely proportional to surface tension). Snapshots at 5 instances of time are shown for each Weber number.

Engineering Visualization Lab

M. Loomis, R. M. Sharpe, K. Mish

Our goal was to establish a venue in which to highlight the work of LLNL's Engineering personnel. We would accomplish this by creating an appropriate space, assembling the necessary hardware and software, and providing visualization expertise for the production and presentation of high-quality audio/visual media. At the close of the project's first year, the Engineering Visualization Lab (EVL) has realized its initial goals.

As a presentation theater, the facility integrates a large projection video screen and surround audio system, with a number of media sources, including computer display output, digital disc recorder, VCR, DVD, and a video network feed from LLTN. Presenters can easily patch a laptop computer into the system or use the resident hardware to display their material on the large display.

The room provides seating for 10 to 15 people, and provides an unclassified environment suitable for small-group collaborations, software demonstrations, or video presentations. High-end animation, compositing, and image processing software staffed by knowledgeable operators provide tools and expertise.

The presentation system is based on a large-screen, rear-projection, video cube and a SGI Onyx 2 computer, which is located in an adjacent machine room to isolate noise and heat. These units were then interfaced with a rack of conventional analog and digital video equipment, and video routing hardware was added to manage signal flow. An Apple G4 computer was added later and integrated into the system for display on the large screen.

Production and authoring software allow the creation of engineering video presentation material in analog or digital formats. A suite of software provides the cornerstone of this capability with an open-ended

and flexible 3-D animation solution. The resulting video can be output as conventional VHS videotape, digital formats such as Quicktime, or DVD media.

A list of key hardware and application software appear below. "Before" (artists conception) and "after" (end of initial hardware integration) images of the EVL are shown in Figures 1 and 2, respectively.

Hardware:

Computer 1	SGI Onyx 2
Computer 2	Macintosh G4
Large Screen Display	Clarity Visual Systems Lion
Digital disk recorder	Accom WSD 2Xtreme
S-VHS video recorder	Panasonic AG-1980
Video Monitor	Panasonic BT-H1390Y
DVD player	Panasonic DVD-A120
Surround sound speakers	Klipsch Synergy 6
AV Receiver	Denon VR-3300
Video switcher	

Software:

3-D Animation	Alias/Wavefront Maya
Compositing, Image Processing	Alias/Wavefront Composer
Video Editing	Apple Final Cut Pro
DVD Authoring	Apple DVD Studio Pro
Format Conversion	Equilibrium DeBablizer
Digital Video Compression	Terran Media Cleaner

Our primary plans for the future are to generate representative content to demonstrate the capabilities of the EVL, and to prepare materials to assist engineers to effectively use the facility. A general distributed platform communication scenario is being developed; a final product would animate the communication paths and integrate simulation data. The goal is to turn large quantities of data into actual *information* that is readily assimilated by a technical audience.

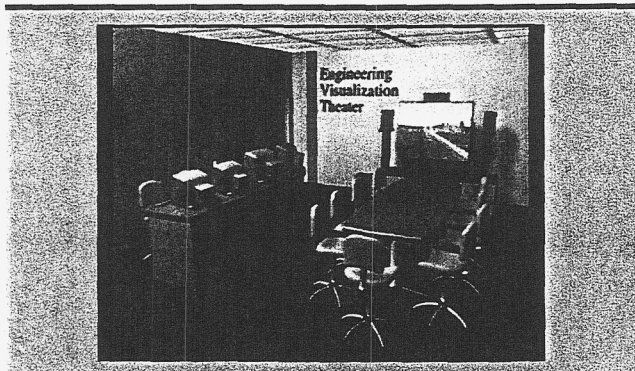


Figure 1. Artist's conception of EVL before this project.

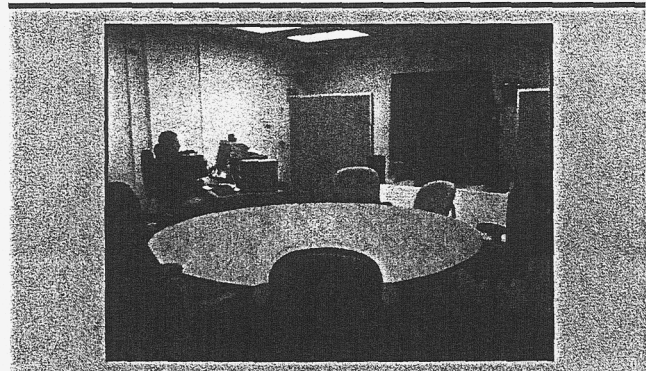


Figure 2. EVL after the initial hardware integration.

Enhanced Fluid Dynamics Capability and Multidisciplinary Coupling in ALE3D

R. McCallen, T. Dunn, G. Laskowski

The objective of this project is to provide an improved modeling capability by incorporating an incompressible flow module in ALE3D, a multi-physics hydrocode developed at LLNL. This addition, coupled to its structural, heat transfer, and chemistry models, will push us into previously unattainable areas of computational modeling.

The need for robust multidisciplinary modeling tools is increasing. ALE3D provides many of the physics options required, but not all. The ALE3D code is at the forefront of multi-physics modeling.

Low Mach number flow is one area where model enhancements are needed. To address this, an incompressible flow model has been implemented to handle cases where compressible flow modeling is inefficient. With this capability and additional improvements in ALE3D algorithms, many programmatic modeling problems of immediate and future concern can be solved.

The implementation was completed in FY99. Moving towards the goal of multi-physics modeling, the heat transfer model was coupled to the flow during FY00. Significant improvements in turbulence modeling capability, model accuracy, and solution speed were achieved in FY01.

The flow is solved for an Eulerian formulation of the time-dependent incompressible Navier-Stokes equations using a finite-element method. Coupling of the heat transfer model requires the addition of an advection term to the thermal transport equation and a Boussinesq term to the flow momentum equation representing the buoyancy force. The temperature is solved independent of the flow equations.

The resulting matrices for the flow and heat transfer equations are assembled using the Finite Element Interface (FEI) developed by Sandia National Laboratories in collaboration with LLNL. The system of equations is solved using the HYPRE parallel solver package developed at LLNL's Center for Advanced Scientific Computing. The library packages allow the use of many advanced iterative linear solvers and preconditioners designed for efficient matrix solutions on massively parallel computer systems.

Significant improvements in speed were achieved by implementation of a pressure stabilization option; an A-conjugate acceleration (or minimum residual projection) scheme; and a linearized implicit time integration

method; and by allowing for the reuse of the static matrix in the FEI. As shown in Figure 1, the pressure stabilization adds coupling between neighboring elements. This improves the solver speed of convergence by reducing the number of iterations. Stabilization also allows the use of fast algebraic multi-grid solvers.

Accuracy improvements were recognized through algorithm reformulation that provided flexibility for the addition of full spatial integration of the matrix coefficients.

The turbulence modeling capability was enhanced with the addition of a one-equation Reynolds-averaged Navier-Stokes (RANS) model called the Spallart-Allmaras model.

These code enhancements were validated by simulating several flow geometries that have characteristics of common engineering flow applications. For example, the code was found to accurately capture the separating, time-dependent flow past a circular cylinder as shown in Figure 2.

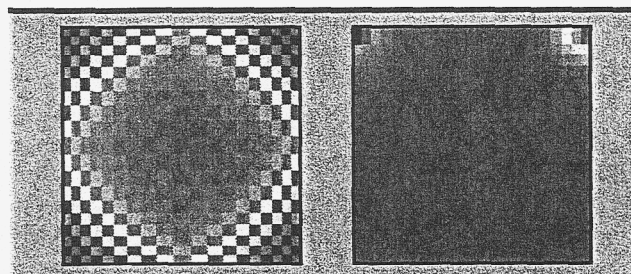


Figure 1. Simulated pressures for a lid driven cavity (a) without stabilization and (b) with stabilization.

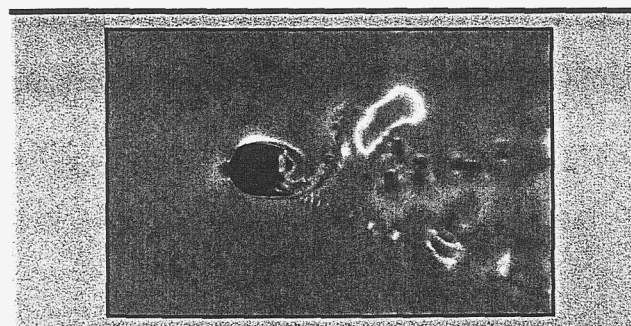


Figure 2. Simulation capturing the time-dependent vortex shedding past a circular cylinder.

Planning Tool for Site Remediation Simulation

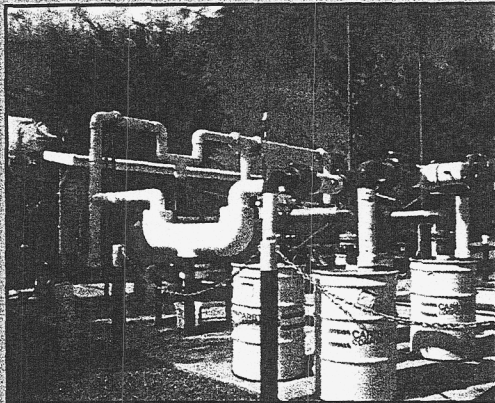
J. Stewart, R. Glaser, A. Lamont, A. Sicherman, T. Hinkling

Site Remediation Simulation (SRS) is a computer-based decision aid and predictive model for site remediation. This management tool is designed to assist site managers and DOE HQ with environmental planning and budgeting. It is designed to optimize budget allocations, level of expertise, technological investment, and consequences of low-probability, unexpected events.

SRS selects the optimal remediation strategy for a given set of constraints. It specifies when to start treating an area, the type of action to take (e.g., pump and treat, excavate, investigate) and the intensity of the application (e.g., how much to excavate, the rate of pumping, the number of wells). Users of SRS can change treatment plans, budget, and regulations to determine other possible scenarios.

The SRS model has been adapted for network use to allow remote sites to operate the model. Each site can be given access to another site's database and operate SRS. The SRS tool facilitates budget negotiations using transparent data and assumptions for the first time in environmental management. It also reduces the response time to a DOE request for a clean-up plan, from days to minutes.

This technology can be used in any long-term clean-up such as a Superfund site. The model (see figure) has been or will be presented to the following: 1) DoD environmental conference in May 2002; 2) EPA conference in May 2002; 3) Japanese chemical weapons excavation and clean-up project managers, January 2002 and Summer 2002; and 4) Petroleum Environmental Research Forum, February 2002.



Components of Model

Physical Sub-Model

- Plume concentration, extent, migration

Cost Sub-Model

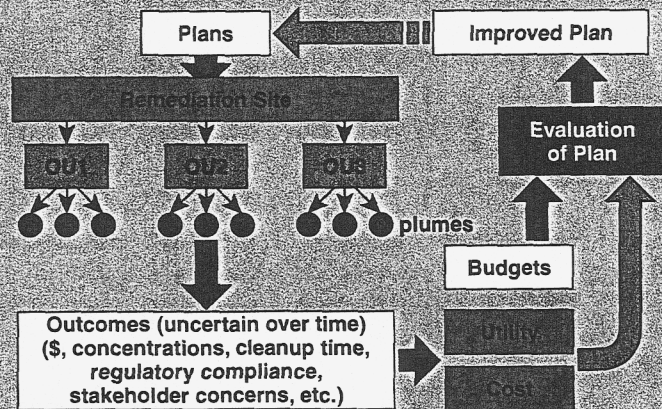
- Short-term and long-term budgets

Planning Sub-Model

- Regulatory and technology selections, expertise levels, research and development

Valuation Sub-Model

- Multi-attribute utility model



Capabilities of Model

Estimates outcomes based on actions

- Outcomes are probabilistic and multi-attribute

Consolidates this information and evaluates plans for decision maker

- Satisfies constraints
- Maximizes expected utility of outcomes
- Accommodates changed conditions

Allows user to test impacts of assumptions

- Uncertainties about the state of nature
- Budget levels
- Technology characteristics

SRS assists decision makers with optimizing complex decisions.

Coupled Engineering Simulation Tools: Solids, Fluids, and Chemistry

C. Hoover, A. Shapiro, R. Ferencz

The Methods Development and Thermal Fluids Groups collaborate on code development for the LLNL finite-element computer programs. The codes model nonlinear thermal and mechanical system responses. In recent years, the LLNL massively-parallel ASCI computers and high-speed workstation clusters have provided the opportunity to extend this suite of codes, NIKE, DYNA, and TOPAZ, with a new generation of computer programs.

Our extended software incorporates multidisciplinary coupling of solid and fluid mechanics, thermodynamics with chemical kinetics, and transport algorithms. The strong algorithm development effort in our groups, supported mostly by the Center for Computational Engineering and technology base funding, focuses on contact interface development, element technology, material models, coupled fluid/solid mechanics algorithms, and chemical kinetics. These activities provide the underlying state-of-the-art modeling capability for the coupled-analysis simulations of the future.

The next four articles in this report detail FY01 progress on these code development activities. The fifth article provides an update on the ParaDyn program, the parallel version of DYNA3D.

The simulation of dams, bridges, and other structures undergoing loads from earthquakes and blasts has been a Laboratory activity for more than ten years. Of particular interest in FY01 were the energy absorption and structural damage predictions resulting from water sloshing against a dam. Significant algorithm development for both NIKE3D and DYNA3D, in collaboration

with the Center for Complex Distributed Systems, gave better predictions for the low-frequency deformation modes of dams.

Chemical reaction kinetics and surface-ablation models have been developed to simulate fuel cells and reentry vehicles. These models are being coupled with finite-volume micro-scale transport models to simulate fuel cells. The TOPAZ3D program has been modified to model surface chemistry by adding finite-volume transport algorithms. These calculations support devices designed and built at the Center for Microtechnology.

The LLNL ASCI program supports our coupled mechanics simulations and parallel algorithm development. Massively-parallel calculations with our production-explicit finite-element program, ParaDyn, can now use a thousand processors with problem sizes up to ten million elements. Representative applications include building designs and retrofits, blast-structure interactions, and full-system weapons simulations with detailed modeling added as needed.

In FY01 we provided DYNA3D/ParaDyn executables to our DoD collaborators. These programs were used to simulate homeland security and other defense-related problems. The challenge to develop massively-parallel nonlinear implicit solid mechanics algorithms is being addressed in our new scalable implicit program, Diablo. This code will grow to encompass simulation of coupled physical phenomena. For example, the surface ablation model prototyped in TOPAZ3D will be included in Diablo. Future capabilities of Diablo will support modeling of the thermomechanical response of weapons and reentry vehicle dynamics, manufacturing, and other processes of Engineering interest.

New Surface Loads and Display Capabilities in DYNA3D

J. Lin

In structural/continuum mechanics problems, a distributed force over a surface area is one of the most common boundary conditions. DYNA3D users can define a surface by a collection of four-noded quadrilateral segments and associate this surface with a specific force function. In the past, the users had two choices for the force functions: a user-input time-pressure table or pressure generated by a user-defined explosive material. In FY00 a third choice, a pressure load module predicting the resistance of soil and underground structures, was added in DYNA3D. The force function choices were further expanded in FY01 to include pressures from hydrostatic, hydrodynamic, and closed-volume gas law calculations. Traditionally, surface loads can be applied only in the direction of the normal to the surface. In the latest version of DYNA3D, surface loads are applicable in directions tangent to the surface.

The hydrostatic and hydrodynamic loading options are for fluid-imposed pressure. The hydrodynamic pressure is based on the classical Westergaard formula for dams with pressure loads arising from ground motion. The user must specify the locations of the dam base and the free surface to have this feature properly activated.

The closed-volume gas pressure load is designed to simulate the pressure variation caused by the volume change of air/gas-filled chambers in a structure system. The possible applications of this feature include the simulation of airbag, piston, gun barrel, and any other compressible fluid-filled enclosure in a structure.

The user must provide a collection of quadrilateral segments that forms a closed volume. DYNA3D calculates

the current volume of the enclosure, based on the Divergence Theorem, and in turn the pressure according to the user-specified gas law. By properly selecting the projection plane for the Divergence Theorem calculation, the algorithm can also accommodate enclosures bounded by boundary surfaces such as fixed boundary plane or plane of symmetry.

Instead of limiting the pressure forces always acting normal to the surface, the latest DYNA3D gives the users the flexibility to apply surface traction in a tangential direction as well. The tangential direction can be defined in a number of ways that are detailed in the DYNA3D User Manual.

With the expanded choices for the surface load sources, the need to be able to display the surface load distribution becomes evident. In the past year, we added the capability, upon users' requests, to have surface loads and contact forces on sliding interfaces included in the DYNA3D output database. During a post-processing session, a user can display either all the surface loads and contact forces, or individual load functions and sliding interfaces separately. The nodal temperature for temperature-dependent analysis and nodal rotational velocities and displacements were also made available for post-processing display.

In addition to the new surface loads and display capabilities, eight material models were either added or upgraded in FY01. Most of these enhancements are an integration of LANL engineers' work. As always in the past and probably for the future years, the maintenance of DYNA3D and its manual, user support, and Collaborator Program Administration are ongoing.

This year, the author also refereed three technical papers for journal publication.

Advances in Implicit Finite-Element Algorithms in NIKE3D

M. A. Puso

The highlights of the NIKE3D implicit algorithm development in FY01 include an infinite fluid boundary condition, contact algorithms, new elements, and an improved hyper-visco-elasto-plastic material model.

A Westergaard added-fluid mass method was developed for NIKE3D to simulate the effects of water sloshing against the surface of a dam (see figure). This method simulates an infinite fluid boundary condition with an added fluid mass discretized at the surface of the dam.

This added-mass algorithm can be used for both a time-domain analysis and an eigenvalue analysis. C. Noble performed an eigenanalysis with this new feature using a model of the Morrow Point Dam and found that the natural frequency of the dam was 50% lower and agreed much better with experimental measurements.

Other new features were added to NIKE3D to facilitate a static fluid force and gravity initialization coupled to a dynamics simulation with DYNA3D/ParaDyn.

Contact algorithms

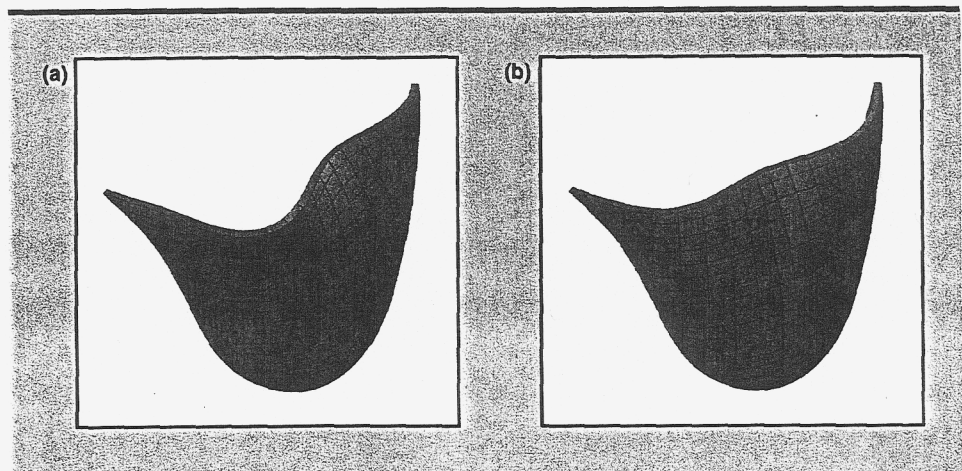
- 1) A new contact algorithm has been implemented with a proper Lagrange multiplier treatment of the contact surface constraint. This method requires a variable number of equations in the linear solver and introduces non-zero diagonal terms and indefinite matrices. Further generalization of the method will be pursued in future work.
- 2) The iterative augmented Lagrangian contact algorithm was modified to allow penalty factor magnification for each

augmentation step. This technique provides tighter gap tolerance control for the interface.

- 3) The contact surface extension algorithm has been improved with better internal logic for choosing the extension length and an input parameter to further influence the surface extensions. The new algorithm prevents spurious contact detection when the extension length is too long.

Element technology and material model development

- 1) A new shell element was developed to replace the default Hughes-Liu shell element. This shell element eliminates the zero energy mode which occurs when point loads are applied.
- 2) Both a C1 beam element and a linear beam element were implemented successfully. C1 beam formulation is often more efficient and robust than C0 beam elements. In addition, the C1 beam elements are consistently linearized and therefore converge better. The linear beam is useful for making comparisons to analytical solutions and for checking model implementation.
- 3) A hybrid-element version of the hyper-visco-elasto-plastic material model was developed. The original version was limited to the enhanced strain element.



Simulation of Morrow Point Dam free vibration: (a) fundamental, and (b) second modes. NIKE3D with added mass feature computes a fundamental frequency of 2.76 Hz, which compares well with the 2.82 Hz computed by Tan and Chopra with a full numerical treatment of the water. The frequency was measured experimentally at 2.95 Hz with a symmetric excitation. This work is part of a study for the US Bureau of Reclamation performed through the Center for Complex Distributed Systems.

Development of Computational Capability for MEMS-Based Technologies

M. A. Havstad, J. D. Morse

Two distinct modeling capabilities have been added to TOPAZ3D in support of both micro- and macroscale fuel cell projects at LLNL. First, an overall reactor rate modeling capability has been integrated into the finite-element structure of TOPAZ3D. Second, a detailed surface chemical kinetic and thermal transport approach is being implemented for microscale modeling.

Our reactor rate work integrates design and thermal management with concepts in LLNL's Microtechnology Center and Energy Directorate. A "plug flow reactor" approach has been mated to TOPAZ3D so that both critical chemical performance parameters (such as fuel conversion efficiency) and thermal parameters (such as start-up or trimming heat) can be calculated consistently.

Our microscale modeling work uses our reentry-vehicle-based surface chemical kinetic effort, and adds detailed transport calculations using finite-volume methods.

A surface chemical kinetic model of a methanol processing microreactor on a chip was exercised, given a flow field solution. Device heat loss, reaction rates, and microheater power were computed. The plug flow reactor approach was also exercised with a similar reactor packed with a porous fuel reforming catalyst. Device fuel conversion efficiency and the evolution of the reactant and product molar flow rates down the length of the micro-channel were computed (Figure 1).

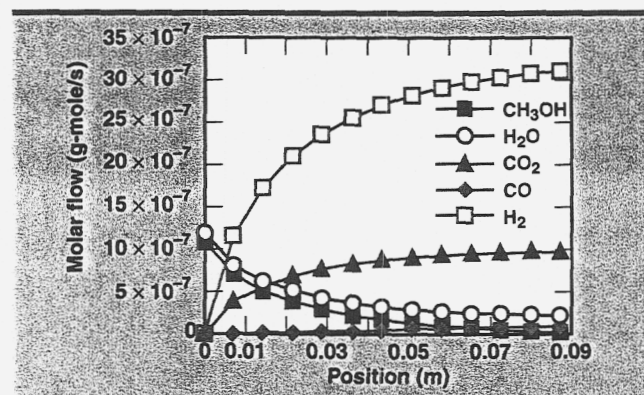


Figure 1. Product and reactant flow rates.

The plug flow reactor approach was also applied to a microscale device fabricated at the Microtechnology Center. Projected thermal performance is shown in Figure 2. Measurements of exhaust gas composition for model validation are in progress. Once agreement is demonstrated, the concept can be scaled up and heat exchange between entering and exiting streams can be optimized.

The detailed transport modeling approach has been built up from a number of capabilities recently added to TOPAZ3D for other efforts (primarily automatic detection of sidelines and mesh rezoning). From these and other efforts it has been straightforward to add the geometric aspects of an unstructured grid finite-volume formulation. Thus the facet areas, neighbor detection, gradient operators, and other strictly geometric items are fully debugged.

Much of the required debugging of the coupled solution of the momentum and mass conservation equations is also done.

Our general and flexible surface chemical kinetic approach has been exercised with six chemical kinetic systems. The coding and input formats allow rapid comparison of the thermal consequences of varying chemical systems. Though this work is motivated by DNT, our comparison of the six systems to data and to other published computations serves as a significant verification and validation effort, applicable to fuel cell development as well.

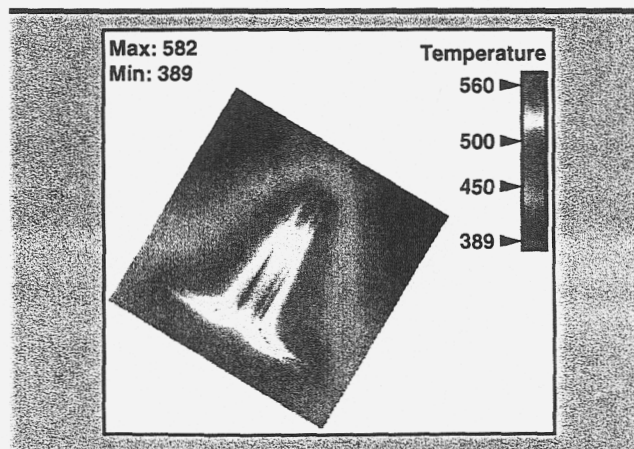


Figure 2. Heated microreactor thermal profile (methanol reformer for fuel cell on a silicon wafer).

Visualization and Data Management Tools: GRIZ4, Mili and XMilics

D. Speck, E. Pierce, L. Sanford

In FY01 there were several major developments in the visualization and data management tools.

GRIZ

The GRIZ User Manual was completely rewritten to document Version 4 changes. It is available online in PDF format on the Engineering network and also through the MDG web page. Several images from the new manual are reproduced below in Figures 1 and 2. GRIZ4 executables are now supported on the Compaq and IBM platforms at the Livermore Computing Center and on Sun and SGI platforms on the Engineering networks.

Feature enhancements implemented in GRIZ include the following: desktop window management has been enhanced to group and display sets of windows for each current execution of GRIZ4; GRIZ menus were enhanced to support multi-dimensional state variable types in the Mili I/O library (Figure 3); both RGB and JPEG image formats can be generated automatically for animations; custom specification of colors used to render mesh edge lines, element outlines, and text and time series plot curves can be selected with the *setcol* command; the *outmm* command from GRIZ2 was ported to GRIZ4; new commands *include* and *exclude* were implemented, which combine the existing functionality of *vis/invis* and *enable/disable*.

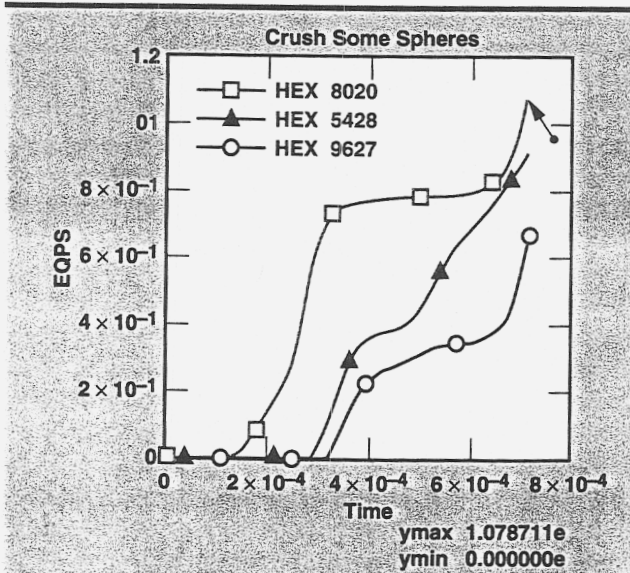


Figure 1. Time history plot of data from Exodus II database, showing cursor coordinates tracking display.

Mili

The XMilics utility was completed and the Mili library has been updated to support IEEE big/little endian format conversions and double precision. Automatic and targeted endian formats are available for Mili databases. This multi-purpose application provides capabilities to support post-processing and restarts of parallel analysis runs.

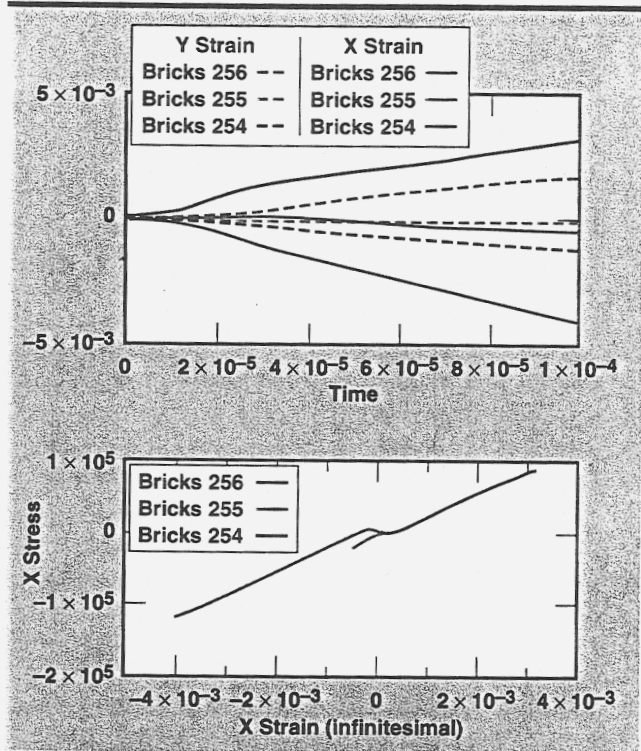


Figure 2. X Strain vs. Y Strain (top) and parametric X Stress vs. X Strain (bottom) for the same three elements.

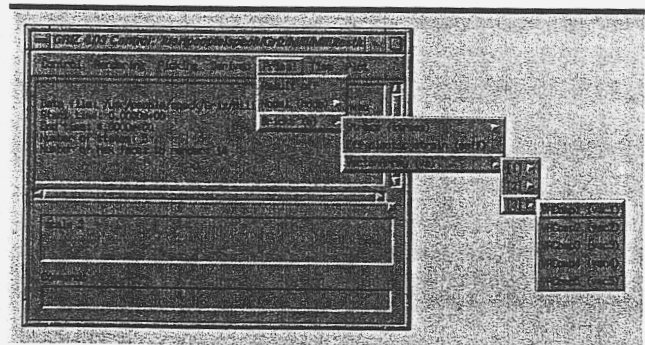


Figure 3. GRIZ menus, illustrating the mapping of a multi-dimensional "vector array" state variable, from a demonstration Mili database into GRIZ's pull-down menus.

ParaDyn Update: Parallel Interface Algorithms

A. De Groot, R. Sherwood, C. Hoover

ParaDyn is an implementation of DYNA3D on massively-parallel, distributed-memory computers. DYNA3D/ParaDyn algorithm design is a team effort involving computational mechanics and parallel algorithm developers. Over the past two years DYNA3D/ParaDyn code developers have collaborated on efficient new methods for modeling contact interfaces. They have successfully designed algorithms for target applications in which materials in the domain undergo large relative motion.

The version 2.x release of ParaDyn represents a significant advance in the parallel contact algorithm capability. The highly optimized parallel contact technique for allocating a full surface to a processor is now complemented with parallel forms of the automatic contact and erosion algorithms in DYNA3D. Analysts can use multiple instances of the automatic contact algorithm to limit expensive contact searches, and these algorithms can be mixed in with the full-surface-to-processor algorithms. Material and domain limiting selection in DYNA3D provide options for optimizing parallel performance.

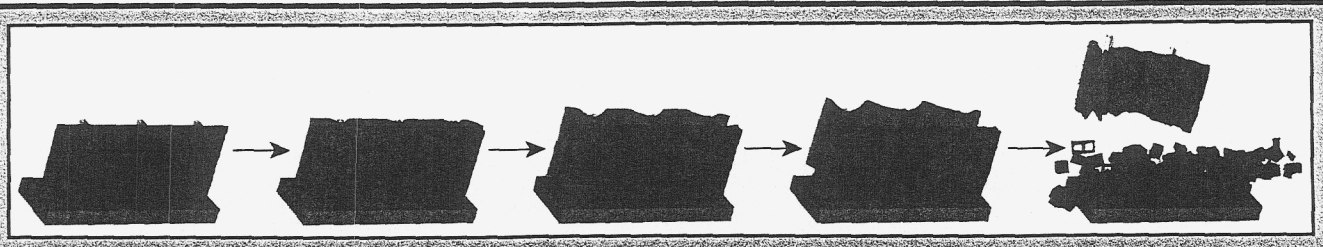
The parallel implementation of the automatic contact algorithms uses a separate domain decomposition for contact surfaces, and includes vertex and edge weights. Dynamic load balancing is implemented to

redistribute the contact surfaces over the processors. Cost functions are used to estimate the frequency for sorting contact surface nodes and redistributing the surfaces over the processors. The initial mesh partitioning is also constrained to allocate nearby interfaces into a single processor as nearly as possible.

ParaDyn calculations for full-system weapons models were routinely carried out on 700 to 1000 processors on the Los Alamos ASCI Blue Mountain system. During FY01 they accrued over 12 CPU years on their system, running ParaDyn simulations to perform sensitivity studies and to generate system response surfaces.

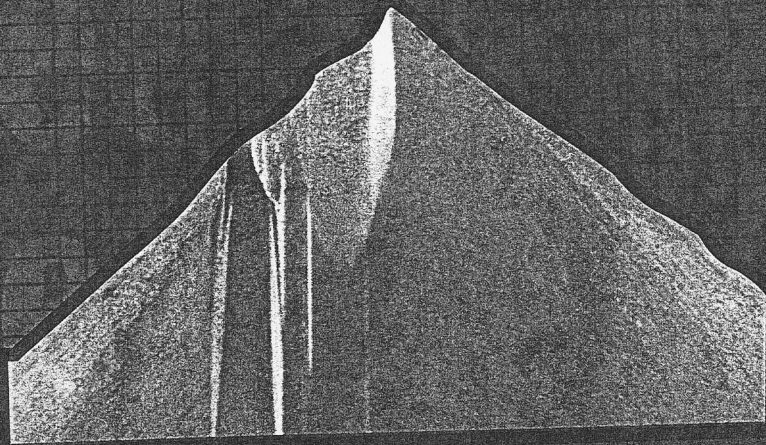
ParaDyn has been used for building design and retrofit applications. The figure illustrates a time sequence of one of several building design simulations carried out by our collaborators at the Army Research Laboratory and the Engineering Research and Development Center. Related calculations model brick and mortar walls with tied-surfaces-with-failure and then use the erosion algorithms to track the debris after failure occurs.

Other algorithm developments completed in FY01 include the parallel implementation of the deformable-rigid material switching and the coupling of ParaDyn analyses with stress-data restart files. These developments in DYNA3D/ParaDyn enable a new capability for modeling manufacturing assembly processes that will be used in future weapons applications.



Time sequence illustrating the collapse of a CMU wall with support posts and a textile liner used in a retrofit design. The ParaDyn simulation for this problem used the parallel automatic contact algorithm with material erosion. The problem size was roughly 500,000 elements.

Center for Microtechnology



UM

Integrated Microsyringe Arrays for Chip-Scale Fluid Control

M. Maghribi, P. Krulevitch

We have developed microfabricated piston arrays capable of controlling fluids (pumping, metering, and valving) in microfluidic devices. Our approach integrates low-power, thermopneumatic sources with piston seals enclosed within microchannels, analogous to microscale syringes. When the pressure source is activated, the metal piston slides within the channel, pumping the fluid on the opposite side of the piston without allowing fluid to leak around the piston. The challenges of this project were fabricating the channels, integrating the pistons, and developing thermopneumatic sources.

A crucial aspect to the development of the microsyringe array is fabricating channels with circular cross-sectional geometry to minimize friction and provide a uniform, leak-proof seal with a spherical or cylindrical piston. We developed an innovative technique for rapidly fabricating circular, smooth channels in polydimethylsiloxane (PDMS), as seen in Figures 1 and 2.

The process is capable of producing channels as small as 30 μm in diameter, but our current microsyringes range from 254 to 508 μm in diameter, due to piston size. These microsyringes can be adapted to meet desired volumetric needs from nanoliters to microliters. The flexible PDMS conforms to an oversized spherical metal piston inserted into the channel, forming a leak-proof seal. This is the reverse of conventional syringes, which use a rigid vessel and compliant plunger.

Reservoirs that contain the actuation fluid were molded along with the channels. The thermopneumatic actuation reservoir is filled with a high-coefficient-of-expansion fluid (Fluorinert 77 from 3M) that is activated by a thin film resistive heater. The heaters are covalently

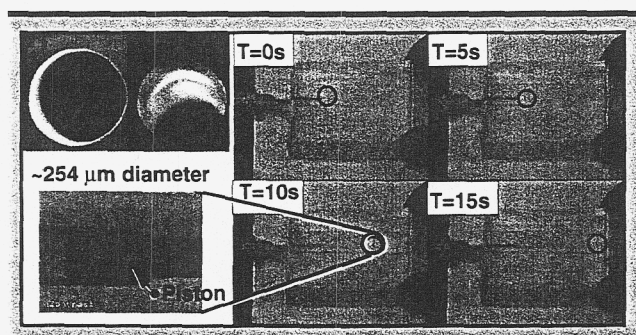


Figure 1. SEM of Microsyringe and time sequence.

bonded to the PDMS containing the reservoirs and channels, using an oxygen surface treatment. PDMS surface treatment in an oxygen plasma produces a hydrophilic surface that is necessary for bonding and fluid loading.

The initial prototype of the microsyringe arrays is shown in Figure 1, along with a controlled time sequence movement of the piston within the PDMS microchannel. Optimal channel diameter was found through multiple iterations to be ~60 to 65% of the piston diameter, to achieve a leak-proof seal without obstructing piston movement within the channel. The pressure requirement to initiate piston movement was between 65 and 100 psi, varying with microsyringe diameter.

These microsyringes offer the capability of truly integrated fluid handling for miniature and field-portable systems. This project has resulted in the development of new techniques that are being used by others, and has also generated a patent application (IL-10630) titled "Low Power Integrated Pumping and Valving Arrays for Microfluidic Systems." This research has also been presented at the Micro Total Analysis Systems 2001 conference in Monterey.

Further funding is being pursued through a number of NIH SBIR proposals, in collaboration with Phoenix Biosciences. All milestones for this project have been completed.

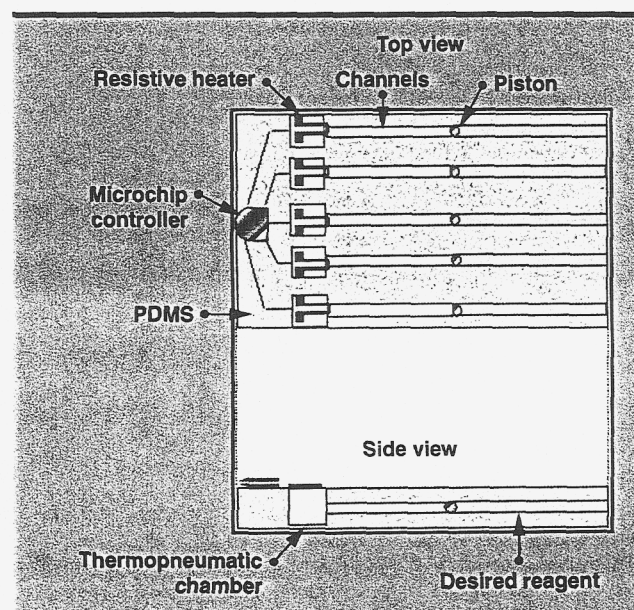


Figure 2. Integrated microsyringe.

Mesoscale NIF and Omega Laser Targets for High-Energy-Density Experimental Science from Nanofabrication

R. Mariella, Jr.

Currently, the targets that are fabricated for High-Energy-Density Experimental Science (HEDES) physics experiments (performed on the Omega laser at the University of Rochester) are hand-made and cannot be fabricated, assembled, and characterized with the precision, accuracy, and throughput that is required. This Engineering TechBase project investigates the use of a focused-ion-beam etching (FIBE) process to address the problem.

HEDES experiments play an important role in corroborating the improved physics codes that underlie LLNL's Stockpile Stewardship mission. A method of material removal and deposition is required that can produce μm -size features on mm-size components in a variety of materials including copper, polyimide, CRF foam, aerogel, and beryllium.

FIBE routinely demonstrates material removal on the sub- μm scale (see figures). The work described in this report is LLNL's first attempt to evaluate the performance of FIBE at commercial/service houses.

In the long term, we believe that LLNL needs to construct a facility, designed from the ground up, to house this capability. Part of this process will be traditional precision machining, but another part will include novel fabrication procedures such as FIBE to remove material with 75-nm precision and accuracy. The use of an ion beam enables a much longer working depth of focus that can be attained with light beams, as well as finer features, in general.

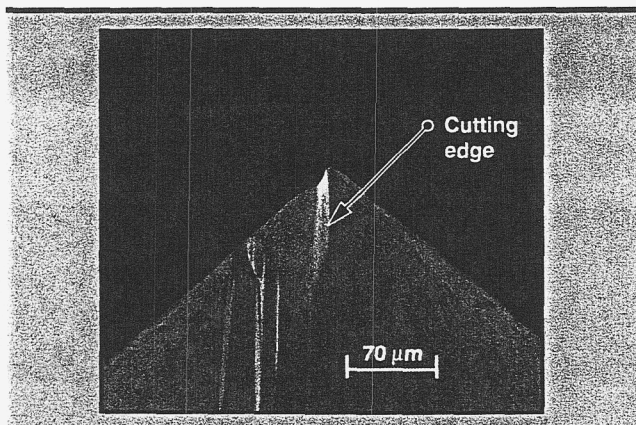


Figure 1. Our first attempt to use FIBE to produce a cutting edge in a diamond tip. This would be used as a precision bit for an end mill.

We have identified and visited four FIBE contractors where we have taken parts to machine.

To evaluate the applicability of FIBE to LLNL problems, we prepared a number of chips with silicon nitride on silicon for etch studies, as well as polished natural diamond tips and EUVL optics (Mo/Si nanolayers on fused quartz).

A few observations became immediately evident, consistent at all four facilities:

1. The manipulation stages are designed to support only the silicon-integrated-circuits industry, *i.e.*, they have precise x-y motion only.
2. All four facilities handled all samples in unfiltered air, and surfaces quickly became contaminated with dust.
3. No facility had SEM on the same chamber as the FIB.
4. On the positive side, sub-10-nm beam diameters are available, and remarkable precision can be achieved in the etching.
5. Specialized 3-D deposition of platinum or other metals is possible.

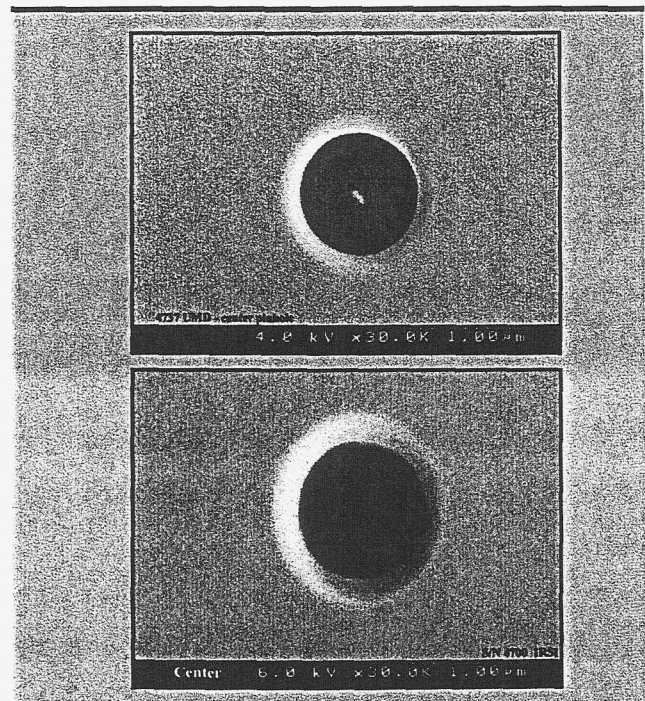


Figure 2. SEM micrographs of pinholes etched into the EUVL optics.

Microstereolithography for Fabrication of Mesoscale Structures with Microscale Features

V. Malba, A. F. Bernhardt, C. D. Harvey, L. Evans

High-energy-density experiments performed with the new NIF facility will play an important role in corroborating the improved physics codes that underlie LLNL's Stockpile Stewardship mission. These experiments will require radical improvements in material removal and deposition methods capable of fabricating fine features on millimeter-size components. We have examined the applicability of microstereolithography (μ SL) to the manufacture of millimeter-sized weapons physics targets for NIF.

Stereolithography is a rapid prototyping technique used commercially to produce macroscale 3-D polymer structures by laser exposure of a photo polymerizable liquid resin in successive layers. Current technology uses a laser focused to a few hundred microns. The size limitation of the technique results from the laser wavelength, the quality and characteristics of the focusing objective, the dynamic control of laser fluence, and the accuracy and repeatability of the mechanical stages.

Our project plan was to convert an existing laser pantography system to a μ SL system by the addition of a z-elevator stage, the retrofit of optics components for 351-nm light, the reduction of the laser spot size, and the repair of the laser.

Of the photoresin materials we evaluated, the best (1,6-hexanediol diacrylate with 4wt.% benzoin ethyl ether as sensitizer) was used to produce a resolution pattern with 10- μ m lines and 10- μ m spaces (Figure 1), the limit of resolution of optics.

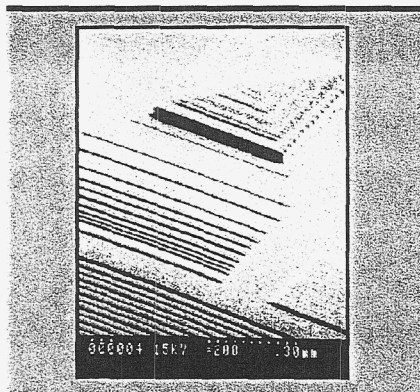


Figure 1. Resolution pattern. The multilayer pyramidal structure clearly shows overlap seams.

Multilayer structures were also fabricated (Figure 2), and considerable effort was directed toward reducing the z-axis layer thickness. The minimum layer thickness achieved was 10 μ m. We are currently experimenting with 1- to 3- μ m lines and spaces with an *ad hoc*, replacement arrangement.

The smallest feature size that can be formed with a photopolymerization system is the product of the diffraction limit of the optics times the solidification factor of the resin. The smallest spot size is given by the diffraction limit ($d = 2.44 \lambda / F/\#$, where λ is 351 nm). For a "fast" objective ($F/\# = 1$), the smallest spot size would be 856 nm.

The solidification factor is the fraction of the exposed volume that is actually solidified. The ultimate resolution of a system with a 0.5 numerical aperture (NA) objective is $856 \times 0.8 = 685$ nm.

An objective with a NA of 1.0 could theoretically produce a polymerized voxel 343 nm in diameter. However, UV optics that perform near the diffraction limit are almost impossible to find, and are difficult to use because of the short focal length.

The resolution of a photopolymerization system is also dependent upon voxel overlap. Even the most carefully controlled motion equipment is hard pressed to provide seamless stitching of voxels. Seams result in unintended surface features that limit the surface finish of the part.

The present system handles the drawing of all features as rectangles, which leads to stair-step lines and jagged-edged circles, which result in features that are out-of-spec dimensionally. We have purchased modern DSP-based motion controllers, to be configured in FY02.

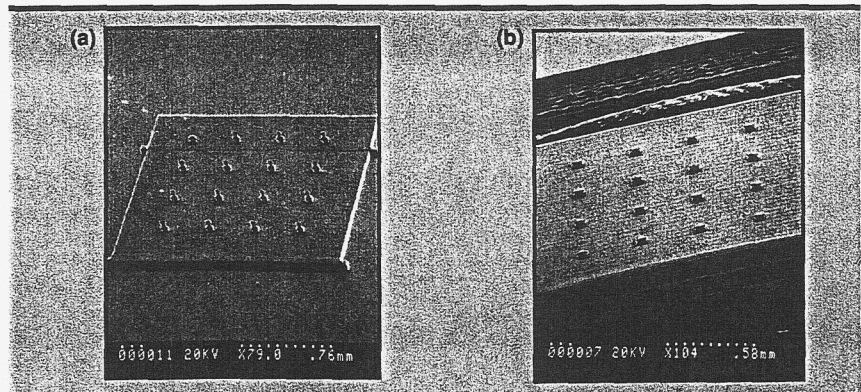


Figure 2. Four-by-four arrays of (a) high- and (b) low-aspect ratio multilayer structures.

Optical Coating Technology

D. Sanders, J. Wolfe

In earlier work, sponsored by NASA, we were able to demonstrate a durable silver coating with an average reflectance of greater than 94%, from 280 nm to greater than 2500 nm. Due to equipment limitations, we were limited in our ability to coat parts larger than 6 in. in diameter. The focus of the current effort was a modified coating process that would allow us to coat larger mirrors with the same formulation, without the need for significant capital equipment expenditure. We were able to demonstrate this new capability by successfully coating a 22-in.-diameter optic under a subsequent contract from the Keck Observatory.

To obtain adequate coating uniformity without the use of uniformity masking, we used a computer model that allowed us to site our deposition sources in the correct locations with respect to the part to be coated.

In addition, we introduced an ion source to enhance deposition energy at the substrate surface. Such an enhancement was necessary to compensate for the reduction in energy of the deposition species that resulted from the increase in source-to-substrate distance. We found we needed to increase the source-to-

substrate distance to allow us to achieve coating uniformity and adequate optical properties simultaneously.

The layout of this successful configuration is shown in Figure 1. The system consists of three 6-in.-diameter sputter sources, an electron beam evaporation source, and a linear ion gun.

After making the modifications, we carried out a series of experiments to convince ourselves that we could reliably repeat our coating process on a 21-in.-diameter part. Once we satisfied ourselves that we could meet both uniformity and optical specifications, we accepted the mirror from Keck Observatory and coated it, along with two witness samples mounted at the perimeter of the substrate fixture.

As can be seen in Figure 2, which represents the actual reflection spectra measured on these witness samples prepared at the same time as the Keck mirror was coated, our approach for coating a relatively large part with small sources proved to be successful.

We conclude from this experience that it is possible to coat larger parts with smaller sources if the magnetron-to-substrate is increased, and a suitable ion source is used to supply an appropriate energetic environment at the substrate surface.

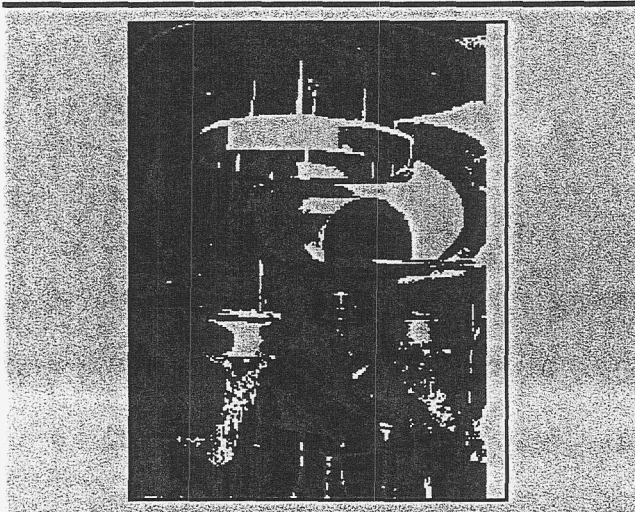


Figure 1. Photograph of successful single rotation layout with Keck part in place.

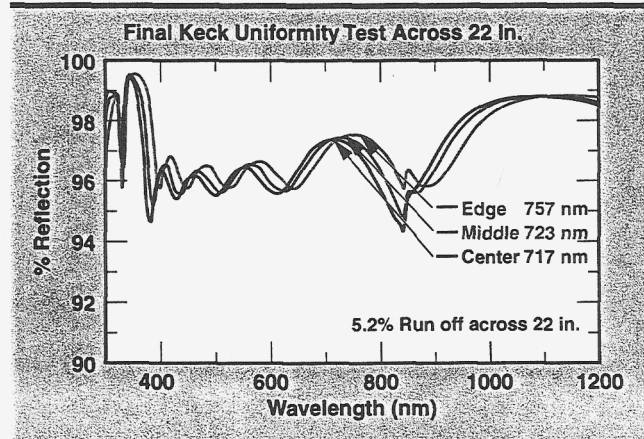


Figure 2. Spectra of witness samples prepared during the deposition of the Keck mirror.

Optical Pressure Sensor

M. D. Pocha, R. R. Miles, G. Meyer, T. C. Bond

The purpose of this technology-base project was to explore the feasibility of a pressure sensor, based on the coupling or modulation of light in optical waveguides embedded in a plastic film.

The problem to be solved is to develop an array of sensors that can be placed between two hard objects under load, and measure the pressure distribution without significantly changing the existing geometry of the objects and their mounting frame. These objects are nominally 25 to 30 cm on a side, or 25 to 30 cm in diameter.

The idea for this project was to embed waveguides in Mylar and use changes in index or dimension to measure the effect of pressure on the phase, amplitude, or other parameters of light propagating in the waveguides.

A series of theoretical and experimental tasks was carried out to explore the original concept as well as new ideas. What is needed is a linear, repeatable sensor that is imbedded in the polymer and will measure its behavior in terms of pressure redistribution over time

without affecting that behavior. We have found a potential solution in silicon-based pressure sensors.

Figure 1 shows the overall geometry for two $6\ \mu\text{m} \times 6\ \mu\text{m}$ waveguides spaced $4\ \mu\text{m}$ apart; Figure 2 shows how the sensitivity of the spacing changes as the gap between the waveguides changes. We used a compact, and extremely sensitive read-out scheme with a Fizeau interferometer to read out a Fabry-Perot cavity gap to an accuracy of ± 1 to $2\ \text{nm}$.

An experiment was designed to measure the gap change of a thin film of plastic on a glass substrate. A large number of measurements were made over several weeks. A typical measurement result is shown in Figure 3.

One outcome of our study was that a more sensitive sensor material would be beneficial. Several of our concepts could be developed into a measurement system, but they all suffer from the nonlinearities of the response of plastic materials to pressure. These sensors, if calibrated, can be used for short-term measurements.

While the initial work looks promising, there is a great deal of additional work to be done.

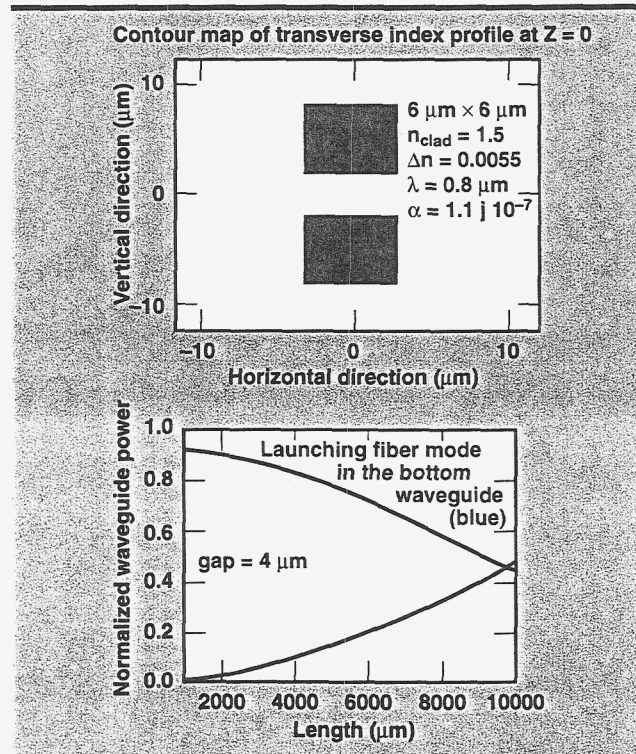


Figure 1. Overall geometry for two $6\text{-}\mu\text{m}\text{-}\times\text{-}6\text{-}\mu\text{m}$ waveguides spaced $4\ \mu\text{m}$ apart.

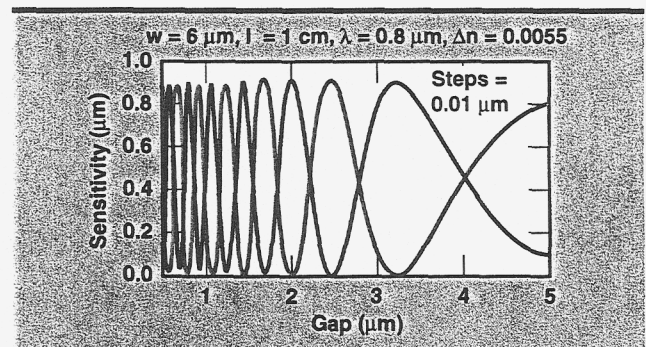


Figure 2. Effect of reducing gap.

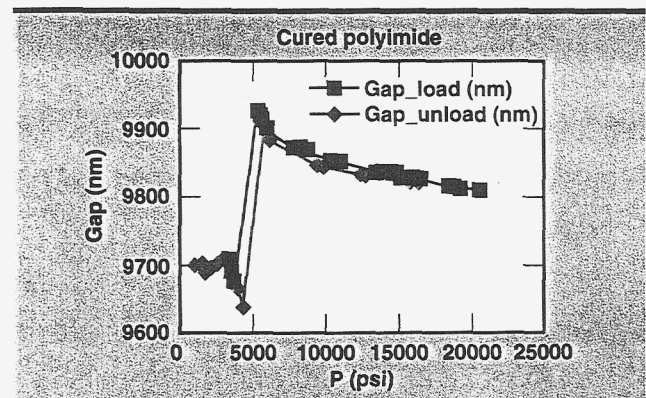


Figure 3. Typical polyimide thickness vs. pressure measurement.

Process Development for High-Voltage Photovoltaic Arrays

G. Cooper, N. Raley, T. Graff

We have worked on device designs and processing techniques that can be used to fabricate high-voltage arrays of photovoltaic diodes in gallium-arsenide (GaAs) materials. Of particular interest to us is the need for low-resistance electrical contacts for both N-type and P-type GaAs.

Many unusual processing problems had to be overcome this year to make progress towards our technical objectives.

The overall device fabrication requires that our diodes be isolated as physical mesas to sustain the generation of more than 1000 V. Using our sputtered metal deposition process (which should be able to bridge across the projections on the sidewalls of our GaAs etched mesa structures) required the development of a metal etch process to remove the metal from the unwanted areas. The metalization we had chosen was a variation of the Ti-Pt-Au metal used successfully on GaAs in the past. Our variation was to remove the Pt layer because there is no simple method to etch Pt without attacking the other layers.

We chose buffered HF for the etchant, despite the fact that it will slowly etch our oxide layer, because of its high etch rate for Ti and zero effect on the GaAs or AlGaAs layers. We completed a test wafer using the Spire, Inc., device designs with the sputtered metal process. Although we achieved good electrical continuity across the sidewall protrusions, the electrical performance of the devices and arrays was disappointing.

We also pursued alternate mesa etch processes, hoping to eliminate the sidewall protrusions and enable a return to the lift-off metalization technique. The most unusual effect we observed is that the age of the citric-water solution greatly affects the etching characteristics of the 30% AlGaAs. We have determined empirically that 26-day-old citric-water solution provides the smoothest sidewalls.

We were also able to show that agitation of the etch solution while etching produces more protrusions on the sidewalls. We believe that this is due to the different etch rates of different crystal planes. We observed that the protrusions seem to be faceted and corresponded to known crystal planes in GaAs.

We also learned that while 80% AlGaAs worked very well as an etch stop and could be easily removed in hot, concentrated HCl, 30% AlGaAs did not provide as much selectivity and was not as easily

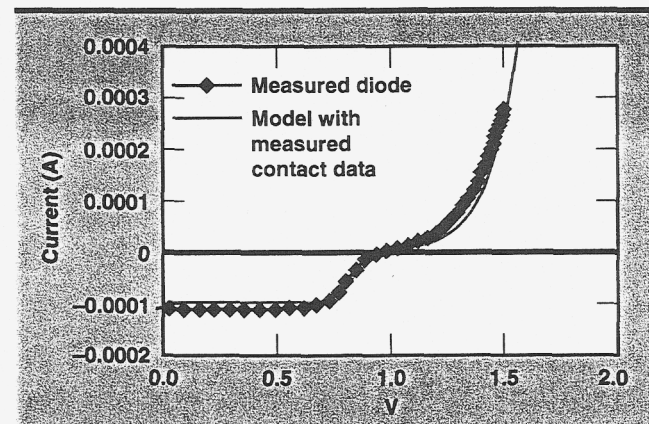
removed. It was around this point that it became clear that there were fundamental problems with the Spire, Inc., array design.

We developed test chips, the most important contribution of which was to verify a fundamentally different and easier-to-fabricate diode design. Diodes fabricated using the new design showed very good light and dark current-versus-voltage (IV) characteristics. Actual N-type contact IV data from the test chip was incorporated into a diode simulation model that produced diode IV curves that very closely matched the IV curves we measured on the test chips (see figure).

Although we feel we can improve the N-type contact and eliminate the "knee" in the IV curve, we believe the existing characteristics are sufficient to meet the demands of our near-term objectives. We did, however, examine the characteristics of AuGeNi contact metalization in case it was required to reduce the N-contact resistance. The N-type resistance with this metal system was four orders of magnitude lower than that achieved with CrAu, as we expected, but there were adhesion problems on the oxide layer.

Using the data obtained from the test chips and the diode model, we were able to design a new array of diodes, currently being fabricated into testable circuits.

Future plans include an examination of 1) AuGeNi metal adhesion on oxide; 2) why citric-water mixtures change over time; 3) the behavior of sulfuric-based etchants when not agitated; 4) maximum doping levels achievable in the LLNL MOCVD growth system; 5) other etch stop layers; and 6) the 80% AlGaAs - GaAs interface.



Comparison of IV data measured on a single test diode under laser illumination with a mathematical model that incorporates real, measured, nonlinear N-contact data.

Rapid Fabrication of Microfluidic Devices by Replica Molding of Polydimethylsiloxane (PDMS)

L. R. Brewer, K. Rose, O. Bakajin, P. Krulevitch

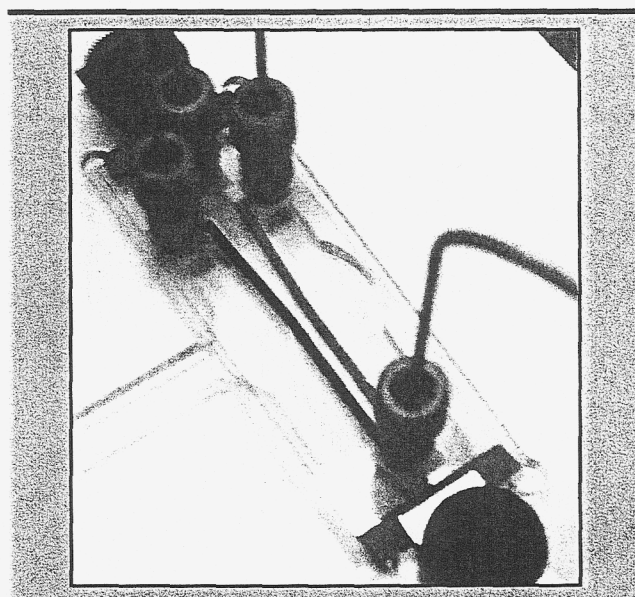
We originally proposed constructing multichannel laminar flow cells for single DNA molecule-protein work from replica molded polydimethylsiloxane (PDMS) because of its many appealing properties, including ease of fabrication, low fluorescence, and optical transparency. However, for our application, there were some unforeseen difficulties, and instead we pursued an alternate approach that was previously demonstrated by Bakajin.

The multichannel flow devices fabricated for our original proposal were not structurally rigid enough to maintain the sub-micron positional accuracy (along the microscope optical axis) necessary for DNA force measurements using optical trapping. In addition, we were not able to fabricate a fluid interconnect that was leak-tight under pressure.

For our alternate approach, a thin (<10 μm) layer of PDMS was spun onto a microscope cover slide and activated in an oxygen plasma. It was bonded to glass into which channels had been wet-etched 40 μm deep. Modified Upchurch fittings, used as fluid interconnects, were attached to the glass using a sheet-like thermal epoxy (Ablestik). The resulting device was structurally rigid and the fluid interconnects did not leak even under high pressure.

Perhaps the most exciting aspect of this technique is that materials with different thermal expansion coefficients can be bonded together because the bonding occurs at room temperature. We constructed a three-channel flow cell, shown in the figure. Red and blue food dyes were injected into the outer channels using a dual syringe pump, and water was injected into the middle channel using a second syringe pump. There was very little mixing between the channels even at relatively low flow speeds (100 $\mu\text{L/h}$). We can now easily fabricate many different configurations of flow cells using this technique.

Future plans include incorporating a micropipette into the flow cell for holding 1- μm beads attached to DNA molecules by applying suction. We anticipate that it will be easy to insert the pipette into a channel machined into the cell and backfill it with PDMS. We plan to replace the syringe pumps with a pressure manifold and high-resolution pressure regulator. Compressed nitrogen will move different liquid constituents into their respective channels with exactly the same force. This will allow for very stable operation of the cell.



A three-channel laminar-flow cell with red and blue dye flowing in the outer channels and water in the inner channel. The depth of the device is 40 mm; the width of the individual channels before they join is 1.5 mm.

Remote Hydrogen Sensor

D. R. Ciarlo

Preliminary results have demonstrated the feasibility of a novel remote hydrogen sensor. The sensor makes use of a bi-morph structure consisting of a 1.4- μm -thick palladium film on a 200- μm -thick strip of glass. In the presence of hydrogen, a stress is chemically induced in the palladium film, causing the glass to bend. This bending is measured remotely, either with optics or radiography.

The remote detection of hydrogen generated inside a closed container is an important problem that occurs often in scientific, industrial, and military apparatus. Hydrogen is a by-product of the deterioration of organic components and it needs to be detected at levels of a few ppm and above. This problem can be readily solved if a tube can be inserted to periodically extract gas for analysis. However, such openings are not always permitted.

The hydrogen sensor in this work can detect hydrogen inside a closed container without any physical access or at worst with the use of non-electrical fiber optics.

The operating principle for this sensor relies on the behavior of a bi-morph structure. One element of the bi-morph reacts with hydrogen; the other does not. The reaction causes a chemically induced strain, which bows the bi-morph structure. This action is similar to the behavior of a temperature-activated bi-morph. The difference is that for this sensor, the strain is chemically, not thermally, induced. The sensitivity of the sensor is determined by the selection of materials and by the size and shape of the elements. We decided to use palladium (Pd) for the reactive component since it is known to readily absorb hydrogen to form palladium hydride (Pd_2H).

One way to remotely read out this sensor is to use radiography. The resolution of radiography in a high contrast environment is 10 to 20 μm . If the contrast is low, as it would be when looking through other material, the resolution is only 75 to 100 μm . This resolution can be improved by using high contrast beads and/or by using a set of bi-morphs, attached at their ends so that gaps are measured.

During FY00 we performed a number of experiments to test the feasibility of this sensor on bi-morphs shown in the figure. We used type 0211 borosilicate glass for the unreactive element of the bi-morph. The

glass was 200 μm thick, 0.5 cm wide, and 4 cm long. For the reactive metal we chose 1.4- μm -thick Pd films because of the known reaction of Pd with hydrogen. Following the deposition, the Pd film was clearly in a state of tensile stress as could be seen from the direction of bow in the glass substrate. The radius of curvature for the bow was 0.85 m as measured with a laser scanner. The bi-morph was then placed in a 4% hydrogen in nitrogen atmosphere at room temperature for one hour. Following this treatment the film was clearly in a state of compressive stress as could be determined from the direction of bow in the glass substrate. The radius of curvature of the glass substrate was 1.18 m.

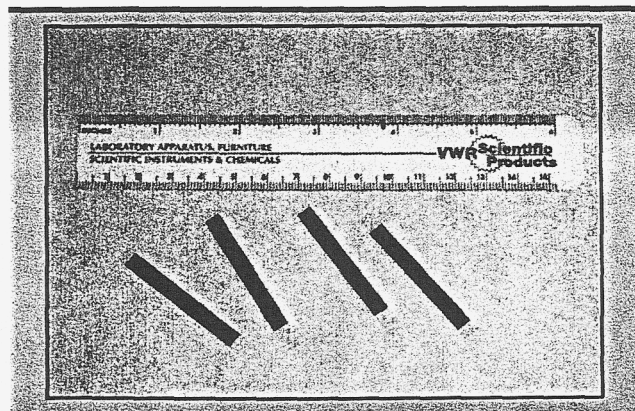
The stress in a thin film on a much thicker substrate can be calculated from the following equation:

$$\sigma = \left(\frac{1}{6RT} \right) \frac{EH^2}{(1-\nu)}$$

where σ = stress in the thin film (MPa), ν = Poisson's ratio for glass, 0.17, E = Young's Modulus for glass, 50×10^3 MPa, H = substrate thickness (m), R = radius of curvature, and T = film thickness.

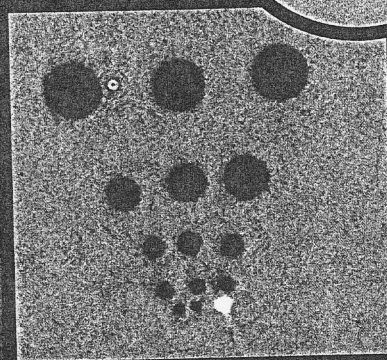
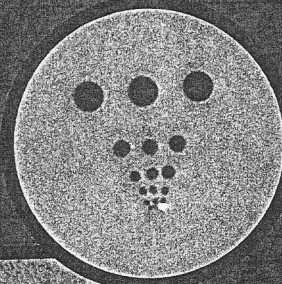
Using this equation, the calculated tensile stress in the Pd film after deposition is 337 MPa tensile. Following the one-hour treatment in 4% hydrogen, the stress in the Pd film was found to be 243 MPa, compressive. The center of the glass strip before and after hydrogen treatment moved a total of 370 μm .

The above experiments demonstrate the feasibility of this remote hydrogen sensor. Further experiments are needed to optimize the shape of the sensor and to calibrate its response.



Palladium-glass bi-morph strips for the measurement of hydrogen.

Center for Nondestructive Characterization



imo

Distributed Processing Algorithms for Reconstruction and Rendering

G. P. Roberson, P. C. Schaich, H. E. Jones, M. W. Kartz

The ability to acquire or generate large volume data sets is currently outrunning our ability to process, analyze, and visualize them. Good examples are the large-volume computed tomography (CT) systems being developed for DOE by the Enhanced Surveillance Campaign (ESC). It is expected that in the next few years these systems will be acquiring data sets that are several terabytes in size, requiring hundreds of processor months to handle. In the past, we have used expensive custom hardware systems that implement graphics-pipe and shared-memory architectures that do not economically scale up as our data sizes increase. Because of this, we have turned to distributed computing systems.

In the last year we have ported three of our heavily used nondestructive evaluation (NDE) codes to a distributed computing system. The small-distributed system that is used in this work was designed to be similar to systems that have been developed by the Advanced Strategic Computing Initiative (ASCI). The goal of this effort is to implement our codes on a scaled-down version of an ASCI type system (~1/300 in size) so that we do not impede everyday operations and we are guaranteed computer time for a process that is interactive and iterative in nature.

We have implemented three codes on our distributed system and have run benchmarks to evaluate their performance. These include two reconstruction codes and one rendering code. The two reconstruction codes include a fan-beam algorithm called the Convolution Back Projection (CBP), and Feldkamp (FDK), an inexact cone-beam algorithm that reconstructs to a limited cone angle. The rendering code is a volumetric ray-tracing algorithm called cell tracer, developed at LLNL.

The CBP algorithm is implemented by transmitting identical code to all the processing nodes (broadcasting) and equally dividing and distributing the projection data. The memory requirement for each node is not severe for this algorithm, as the image slices along the z-axis can be stored onto disk as they are reconstructed. After the reconstruction process, a portion of the volumetric image can reside on each of the processing nodes. This is ideal for further processing of the 3-D

image if it is required. Implementing the CBP algorithm in this way provides code that runs very efficiently on a distributed system.

We can distribute the problem over a number of processors equal to the number of projections. The number of projections is typically on the order of 1000 to 1500 and will reach 8000 in the near future.

The FDK algorithm is implemented by broadcasting the algorithm and the projection data set to all the processing nodes. The image that is reconstructed is equally divided and distributed over the processing nodes. The projection data is broadcast to all the processing nodes, one projection at a time. The portion of the volume image that resides on each node is updated by each projection as it arrives. Like the CBP algorithm, the volume image is distributed for further processing after the reconstruction.

Memory requirements are higher for FDK than the CBP because the image portion that is being reconstructed must reside in memory to attain an ideal processing speed. The reconstructed image volume can get very large; however, the image is distributed over all the processors and with an increasing number of nodes, less memory is required per node. The FDK algorithm also runs very efficiently on a distributed system. The reconstruction problem can be distributed over a number of processors equal to the number of slices along the x-axis of the image. This number is typically 1000 to 2000 but will soon be 4000 to 8000.

The cell-tracer algorithm is implemented by broadcasting the code and the volume image that is being rendered. Different projections are produced at each processing node. The projections are produced for different angles around the volume image and represent frames of a movie. In this implementation, the memory requirements are severe as the entire image volume resides on each processor node. The algorithm was implemented in this way because of its simplicity, requiring less modification of the code.

We hope to implement a more practical rendering algorithm in the future, where the image is distributed and a portion of each projection is produced by each processing node, thereby reducing the memory requirements per node.

Enhancements in Infrared NDE Techniques

W. O. Miller

Infrared methods for nondestructive evaluation (NDE) are being enhanced as part of the overall LLNL Center for Nondestructive Characterization (NDC) effort. Sonic IR is being pursued with both theoretical and practical efforts. Sonic IR shows promise as a new IR NDE technique that can detect flaws, such as tightly closed cracks that are difficult to detect with other methods. We have successfully evaluated Sonic IR on several materials and flaw types. Quantitative NDC is a new effort that will apply and correlate several NDE techniques, including IR, to evaluate microstructural defects in ceramics.

NDE methods are necessary tools for many programmatic efforts, with applications such as parts certification and materials characterization. IR NDE methods have several unique advantages, including noninvasive and noncontact inspection, portability, simplicity, and relatively low cost. Further, certain material characteristics and flaw types are more readily characterized by IR NDE than by other methods. Sonic IR is a new technique for NDE that works by dynamically exciting the part being tested with an acoustic probe that is in physical contact with the part. Any resulting differential motion across a crack face creates heat by friction, and a traditional IR camera images the transient temperature rise at the crack. We found that the method and equipment used for this study were generally effective for all except the smallest flaws.

The initial effort was to see if Sonic IR could detect small cracks in aluminum oxide. Three types of aluminum oxide coupons with flaws were made. First, surface grinding produced a large field of surface damage of approximately 0.2-mm closed cracks. Second, a Vickers hardness test bit was pressed into the

material to produce a radial array of closed surface cracks, each approximately 1 mm long. Third, notched beams were cracked by three-point bending, producing cracks approximately 4 mm long.

Flaws were imaged in all but the small surface ground defects (Figures 1 and 2). The inability to detect the flaws in the surface ground coupons may be due to both inadequate spatial and temporal resolution of the IR system, and a poor match of input forcing between the acoustic probe and the aluminum oxide parts. Additional effort to resolve this is underway.

Sonic IR tests were made on carbon composite tensile specimens that had been fatigued to failure. The Sonic IR images of the damage areas were clear, and in excellent agreement with ultrasonic images.

New efforts in Sonic IR include studies to examine the response to alternative input parameters (broadband, sweep), and image processing for reconstruction of subsurface detail from surface thermal images.

Qualitative NDC is a new effort that will provide information on microstructural variations in ceramics. A major component of this effort will be the application and correlation of results from several NDE techniques. Passive and heated IR methods will be used to measure local thermal property variations in ceramics in support of this effort.

In FY02 the project will include experiments in a range of acoustic input devices to rapidly reveal flaws of many types while preventing part damage. Signal processing of the thermal images will include efforts in formal deconvolution to reveal 3-D subsurface detail.

The effort in quantitative NDC will include the preliminary investigation of suitable IR techniques, with a focus on the traveling heat source method from NASA Langley.

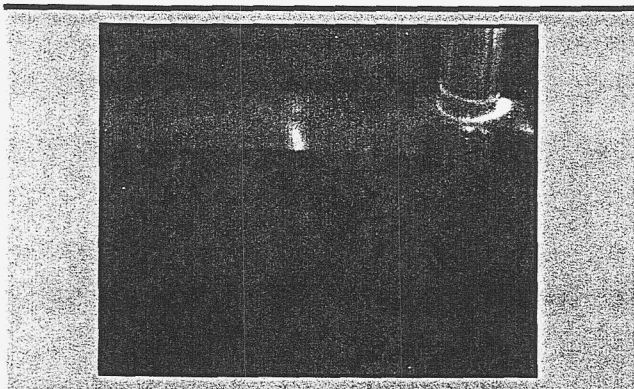


Figure 1. Sonic IR image of a 4-mm crack in a notched beam coupon.

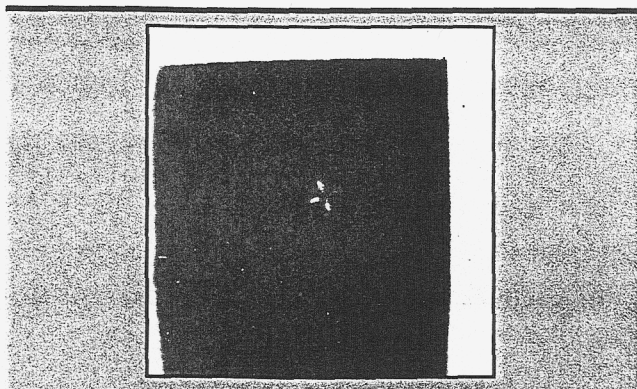


Figure 2. Sonic IR image of four 1-mm cracks in a Vickers coupon.

High-Precision Quantitative Tomography of Mesoscale Targets

W. Nederbragt, S. Lane, D. Schneberk, T. Barbee, J. L. Klingmann, R. Thigpen

High-Energy-Density Experiments play an important role in corroborating the improved physics codes that underlie LLNL's Stockpile Stewardship mission. Conducting these experiments, whether on NIF or another national facility such as Omega, will require not only improvement in the diagnostics for measuring the experiment, but also the fabrication and characterization of the target assemblies.

The characterization of the target assemblies is as important as their fabrication: just as the actual target assembly is the input to the experiment, the characterization of the target assembly is the input to the physics simulation. With this in mind, a radical improvement is needed in characterizing the target assemblies that comprise millimeter-sized components with micrometer-sized features.

X-ray radiography/tomography is one technique that holds promise for characterizing the internal structure of target assemblies. Sub-micrometer spatial resolution has been demonstrated using a synchrotron x-ray source. This approach will accommodate our requirements for a high throughput and low cost approach for characterizing production quantities of target assemblies.

This TechBase project is funding the construction of a Kirkpatrick-Baez (K-B) microscope. This is a classic x-ray optics design commonly used for focusing x rays. It uses two grazing-incidence mirrors. Each mirror focuses the x rays in one direction. Although this microscope does not meet all of our goals, it has a proven track record. It will be a chief resource as we continue to improve our target characterization capabilities.

We are making one improvement over the standard K-B design: we are using multi-layer mirrors to improve the throughput of the instrument.

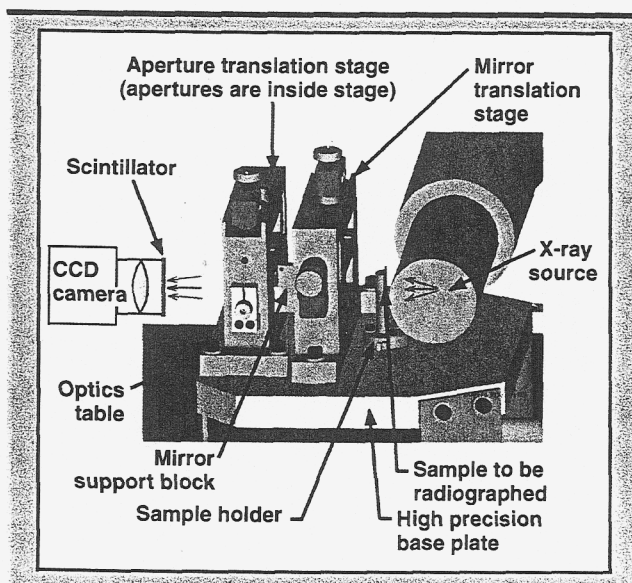
During FY01, we completed the instrument design, fabricated or purchased all of the necessary hardware, and began assembling the system. Most of the year was dedicated to the optical design. Several different variations on the standard K-B design were considered, including the use of extra mirrors and the use of

non-spherical surfaces. We also investigated the performance-enhancing characteristics of apertures when used with the standard K-B microscope. We concluded that the standard K-B with optimized aperture placement was the best choice because of its simplicity and good performance.

After choosing the optical design, we conducted a sensitivity analysis of all of the instrument components to determine the effect of position errors on the instrument's imaging performance. With this information it became apparent that we needed to have four degrees of freedom on the instrument to correct any misalignments created during manufacturing and assembly. The mechanical design (see figure) of the instrument followed the completion of the sensitivity analysis.

The instrument components were fabricated and purchased based on the finalized mechanical design. We now have the majority of the parts in our possession, and we have started the assembly process.

In the beginning of FY02, we will complete the assembly of the instrument and begin using it.



Geometric model of the base of our Kirkpatrick-Baez microscope. The instrument should provide sub-micrometer resolution of an object over a quarter-millimeter field of view.

Linear Array Computed Tomography

K. Dolan, J. Fugina, J. Haskins, R. Perry, R. D. Rikard

The objective of this project was to improve our capabilities for fan beam computed tomography (CT) by adapting new x-ray sensitive, linear diode-array technology to an existing CT platform. A linear array CT system was upgraded with improved digital linear array x-ray camera technology. The new system provides 80- μm pixel pitch with square pixel format, higher detection efficiency, and extended operating range. The linear array system uses collimated fan beam geometry to reduce x-ray scatter noise and increase quantitative analysis capabilities.

Use of fan beam geometry for CT has the advantage of greatly reducing scatter at the detector array to improve signal-to-noise ratio and reduce quantum noise. This is done by slit collimation to limit exposure of the object to just the region of interest.

The new system realizes a factor of 5 improvement in spatial resolution with a 5500-element array at a pixel pitch of 80 μm (6 line sets/mm). It provides a factor of 100 improvement in detection efficiency, which more than compensates for the smaller pixel size, and extends the operating range by a factor of 2 up to an x-ray energy of 450 keV. (External shielding is required above 225 keV.) Readout time per line is 1.0 ms, which is a factor of 4 improvement, even though the new array has 5 times the number of elements.

Image integration time can be varied from 1 ms to 4000 ms, which extends our image integration capability by a factor of 40. The system retains 12-bit dynamic range (4096 gray levels), and 470-mm linear array length. The new system on the existing platform is shown in Figure 1.

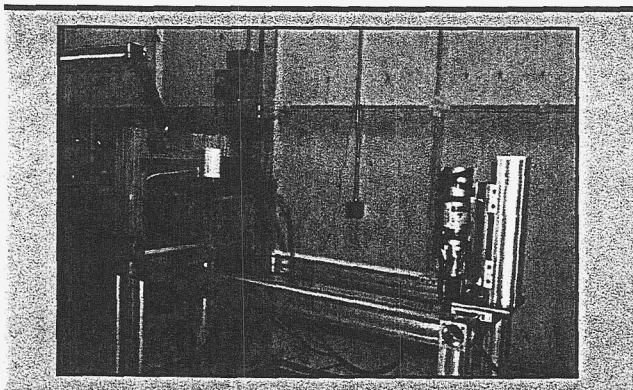


Figure 1. LCAT linear array CT system showing linear array and staging with test object at left, and x-ray tube at right on tubular frame stand.

New capabilities with the upgraded system are as follows:

1) Pixel and Line Binning. Statistical uncertainties can be decreased. Up to 16 pixels or 8000 lines can be combined.

2) Fast Digital Radiography. This mode can perform single radiographs, multiple sequential radiographs at incremented object rotational orientation, or up to 3-D CT data scans.

3) Fast Sinogram. This mode can perform a single sinogram at a desired location, multiple sinograms separated by selected Z-increment distance, or multiple sinograms for sequential Z-axis locations.

4) Increment Average Radiograph. This mode constructs single radiographs or provides up to 3-D CT data sets by obtaining averaged digital radiographs at as many projection angles as desired.

5) Increment Average Sinogram. This mode can perform a single averaged sinogram at a desired Z-axis location, multiple averaged sinograms separated by selected Z-increment distances, or multiple averaged sinograms at sequential Z-axis locations corresponding to projected Y-pixel dimension for 3-D CT reconstruction.

Examples of a digital radiograph and a CT reconstruction obtained with the upgraded system are given in Figures 2 and 3.

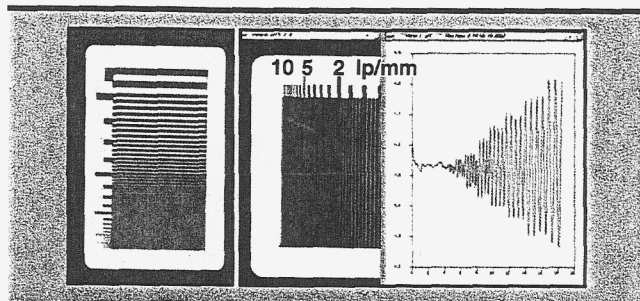


Figure 2. Digital radiograph of line pair gauge (left) and trace analysis (center and right).

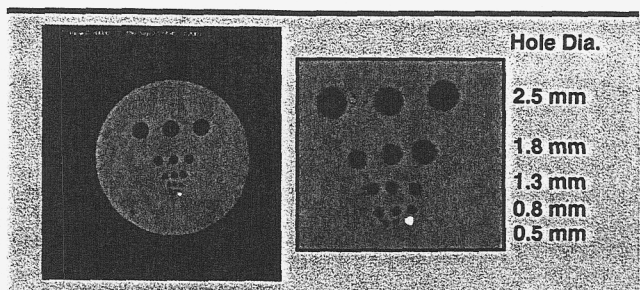


Figure 3. CT reconstruction of cylindrical hole set phantom, full image (left) and enlargement (right).

Neutron Radiography Beam Stop

B. Rusnak

A commonly used method for producing 10- to 13-MeV neutrons uses a deuterium-deuterium (D-D) nuclear reaction: a 7- to 10-MeV beam of D ions from an accelerator impinges on a small volume of high-pressure D gas confined in a vessel. A very thin metal window on one side of the vessel allows the beam to shoot through, but still physically separates the D gas from the vacuum environment needed for the accelerator to run. This approach has traditionally limited the beam intensity to a few μA of average current, which limits neutron production to 10^8 to 10^9 neutrons/s. To image larger, denser objects, we are building a high-power neutron imaging machine that uses a virtual aperture to replace the thin window. We have also determined that using a pressurized high-atomic-number gas beam stop is a viable approach for stopping an intense 7- to 10-MeV deuteron beam.

Our imaging machine, shown in the figure, uses a rotating aperture system — a series of six rotating and stationary disks with small holes — to replace the thin beam window. The holes act as a dynamic shutter system that allows the beam to enter 2% of the time, and is effectively closed to seal off the gas area from the vacuum 98% of the time. While this system promises to increase neutron production by a factor of 20 over windowed systems, it also creates the problem of having to dispose of the more intense beam after it goes through the gas.

Traditional methods of stopping the beam on a metal plate are complicated by very high power densities that would literally blow away a solid metal surface no matter how well it was cooled. If the plate were slanted so the beam was at a grazing incidence, or if the plate were rotating, the resulting mechanical bulk of the device would create more scattered neutrons that would degrade the overall imaging system resolution.

A way to address this problem is to stop the beam in a high-pressure, high-atomic-number noble gas like Xe or Ar. With this approach, there are several advantages: we stop the beam within 8 to 10 in.; we are at or below the Coulomb barrier for the resulting nuclear collision, precluding by-product neutrons or radionuclides; the gas can handle the heat load better than a solid material; the gas is self-healing, since

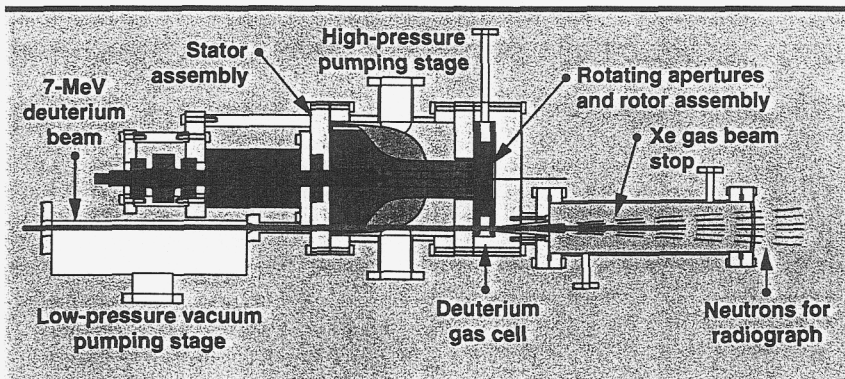
the volume of gas that is heated by the beam and rarefied will re-equilibrate and cool on its own. Finally, having a noble gas contiguous to the high-pressure D gas that is producing neutrons creates a situation where the produced neutrons are nearly monoenergetic, since the beam only transfers about 10% of its energy in the D to make neutrons.

Our objective was to evaluate this concept of using a high-pressure, high-atomic number gas for a high-power beam stop.

A data set was established for the anticipated gases, including D, Xe, and Ar. Using values for the density, the critical pressure and temperature, the thermal conductivity, and the heat capacity as a function of pressure, we estimated the sound speed for the D flowing into the high-pressure vacuum chamber when the apertures opened. Calculations showed if the first and second rotating apertures were separated by a sufficient distance, the advancing gas from the opening of the first aperture could not reach the second aperture before it closed, thereby greatly improving the sealing efficiency of the overall system.

Gas hydrodynamic simulations were started, using the ALE3D code to evaluate how the high-energy particle beam would affect the neutral gas in both the D gas cell and the Xe gas beam stop. Our work has led to a better understanding of the energized beam focus channel hydrodynamics. Implemented design changes based on this work are expected to greatly improve the performance of this system.

The main application for this technology is as a beam stop for fairly intense (1- to 20-mA), fairly low-energy (5- to 20-MeV) particle beams from pulsed accelerators. This technology can also be used for attenuating extremely intense beams of light that come off accelerator-driven coherent light sources.



Mechanical design of the rotating aperture system, the D gas cell, and beam stop.

Rapid High-Resolution Ultrasound Tomography

J. Kallman, E. Ashby, D. R. Ciarlo, G. Thomas

Transmission ultrasound imaging is performed by passing ultrasound through an object of interest and mechanically scanning a point sensor to determine the sound field transmitted. This process is slow, typically taking 20 min per acquired field. We have produced a sensor that currently acquires the acoustic field over the 2-D sensor aperture in 20 s. This, and anticipated further increases in speed, make feasible new uses for transmission ultrasound in nondestructive evaluation and medical imaging. This sensor technology will make possible applications such as near-real-time inspection of parts as they come off assembly lines, and rapid transmission ultrasound tomography for breast cancer screening.

The objective of this project is to speed the acquisition of transmission ultrasound data for tomography through the use of a new kind of acoustic sensor. The Optically Parallel Ultrasound Sensor (OPUS) images an acoustic pressure wave over an entire surface by converting sound pressure into an optical modulation.

The key to this conversion is evanescent field coupling. When light encounters the interface between a slow medium (high index of refraction) and a faster one (lower index of refraction), light is both reflected and transmitted. The transmitted light is refracted as per Snell's Law: $n_1 \sin(\theta_1) = n_2 \sin(\theta_2)$, where n_1 and n_2 are the slow and fast media indices respectively, θ_1 is the angle of incidence, and θ_2 is the angle of refraction. As θ_1 approaches the critical angle θ_c (where $n_1 \sin(\theta_c)/n_2 = 1$), θ_2 approaches 90° and the light that is transmitted decreases. Beyond the critical angle, all the light is reflected.

There is, however, an evanescent field that extends beyond the slow medium and into the faster one. If another piece of slow medium intercepts this field, some of the light tunnels across the gap and is transmitted, with a corresponding decrease in the reflection from the original total internal reflection (TIR) interface. The amount of light transmitted is sensitively dependent on the gap size (by the time the gap is approximately 1 wavelength, the evanescent field has dropped almost to zero).

We exploit this phenomenon by suspending a flexible membrane over the TIR surface and exposing the opposite surface of the membrane to an acoustic medium. An acoustic wave hitting the membrane will cause it to deflect, changing the gap between the

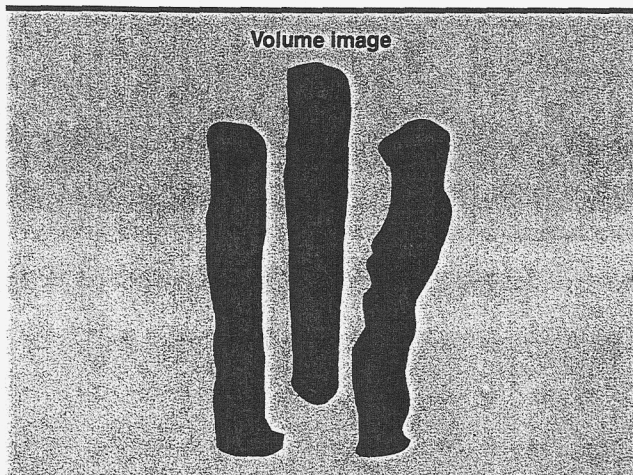
membrane and the TIR surface, and causing a change in the reflection. By illuminating the TIR surface with a strobe light and observing it with a video camera, we can observe and record the membrane deflections.

We have applied LLNL's expertise in computational modeling and microfabrication to the development of the OPUS.

In FY00 we built robust, low tension membranes that produced 0.7-cm-x-0.7-cm sensors that can survive indefinitely; upgraded our camera to speed data acquisition by a factor of 100; acquired multiple views of a 2.5-D phantom; and performed diffraction tomographic reconstructions using these data.

In FY01 we were unable to scale up the aperture on a membrane-based sensor, and therefore were unable to complete our fabrication plans. We investigated a paraxial-wave-equation-based adjoint method for reconstruction with transmission data and were able to use previously acquired data to perform 2.5-D tomographic reconstructions.

In FY02 we plan to examine a new method of fabricating the sensor that will not require suspending a membrane on the optical substrate. This method should be inherently scalable and produce a sensor that is more sensitive and less expensive to produce. We also plan to produce a full 3-D adjoint reconstruction code and to write an invention disclosure on the nonmembrane based sensor design to update the patent awarded in FY00.



Two-and-a-half-dimensional diffraction-tomography reconstruction of phantom. The phantom consists of three pieces of monofilament fishing line, each 0.5 mm in diameter, arranged at 120° intervals on a circle 1.5 mm in radius.

Synchrotron Microtomography at LBNL's Advanced Light Source Facility

K. Dolan, D. Haupt, J. Kinney, D. Schneberk

A microtomography system for nondestructive microstructural characterization and internal dimensioning at small length scales will be installed on the dedicated computed tomography (CT) beamline at the Advanced Light Source (ALS) synchrotron facility at LBNL. We have adapted previously developed LLNL software for the user interface to provide motion control, data acquisition, data transfer, image analysis, and reconstruction.

The ALS CT beamline has two experimental stations being built into shielded hutches, one for x-ray microtomography and one for x-ray microscopy. The microtomography system consists of translation staging, a lens-coupled camera-based imaging system, and data acquisition and control systems. It was designed to obtain spatial resolution as small as 1 to 2 μm in the microtomography hutch with parallel beam geometry at x-ray energies in the range 4 to 100 keV.

The camera-based imaging system is also appropriate for image acquisition in the x-ray microscopy hutch. For this application, the design is expected to provide spatial resolution as small as 0.1 μm with x-ray energies in the range 3 to 12 keV. When translation stages become available in the x-ray microscopy hutch, the imaging and data acquisition systems will be available for microtomography at these smaller length scales as well.

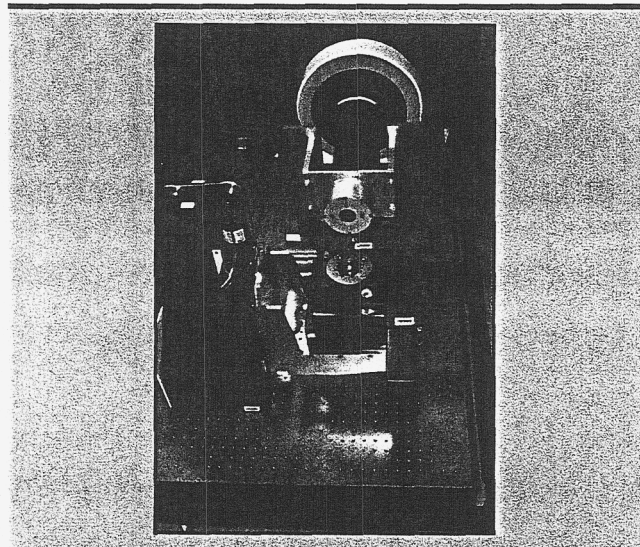


Figure 1. Microtomography system mounted on optical bench showing 3-axis positioning system (front), scintillator mount and extension tube (center), and ring rotational camera mount (rear).

The microtomography imaging detector is based on a lens-coupled design consisting of a cadmium-tungstate scintillator, high-quality optics, and a CCD camera. The scintillator is 50 mm diameter by 0.75 mm thick, and is selected from high-grade scintillator material to be nearly flaw-free. The optics is a high-quality lens tested during a previous program and demonstrated to provide 180 lp/mm. The cooled CCD is a 3-k-x-2-k chip with sensitive elements 9 μm \times 9 μm .

At nominal magnification of 1.0, the system accommodates objects up to 27 mm in diameter and 100 mm vertical, and provides spatial resolution of approximately 20 μm . At the maximum optical magnification of 5.4 provided by the high-quality lens, the system accommodates objects up to 5 mm diameter and 20 mm vertical with spatial resolution of approximately 3 μm . The horizontal and vertical mechanical stage positioning and repositioning accuracies have been verified to be ± 0.5 μm .

The microtomography system as assembled on an optics table for the field work is shown in Figure 1. Examples of CT reconstructions from data taken at SSRL, where the system has been used successfully, are shown in Figure 2.

Significant improvements in image resolution and contrast and extended capabilities are expected since the beam divergence and beam intensity at ALS are both improved over SSRL data by nearly a factor of 10.

Three areas that have benefited from synchrotron tomography, and are in urgent need of the greater precision this beamline will allow are: 3-omega damage studies, shock spallation studies, and NIF target characterization. Other areas will benefit from the monochromatic radiation and high signal-to-noise provided by the ALS synchrotron source, which is expected to come on line in February, 2003.

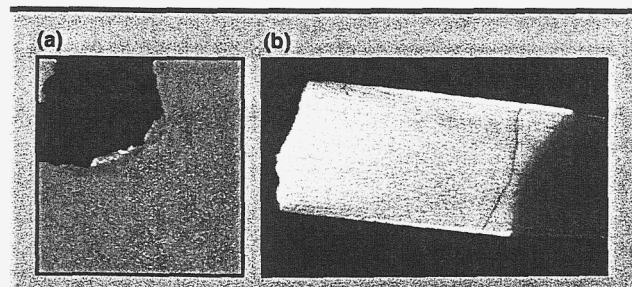


Figure 2. (a) Tomogram of laser beam damage in silica, showing local densification near edges of cavity (white region). (b) Tomogram of composite bond test sample, showing bond depth (mid-tone region between light and dark regions) and microcracks in higher density (light colored) region.

Three-Dimensional Profilometer

M. W. Bowers, D. W. Swift, G. W. Johnson

The primary goal of this project was to show that we could take commercially available telecommunications, cell phone, and survey instrumentation technologies and merge them to build a more accurate coordinate measurement machine. For this we needed to show that it was possible to achieve better than 10- μm measurement resolution with better than 50- μm transverse resolution, and that it was possible to rapidly and accurately scan the measurement beam across the target area to be measured.

Our design (Figure 1) is based on a microwave interferometer. For this system we use an 8-GHz RF source. The RF power is transmitted to a microwave splitter, allowing for the two arms of the microwave interferometer. One arm becomes the reference arm and the other is the measurement arm that is used to measure the distance to a target point.

Since we cannot focus the microwaves down to a small point on the target, we must use an optical frequency as the carrier for the microwaves. We used a telecommunications laser diode at an eye-safe 1550-nm wavelength. The RF power modulates the optical beam using an integral Mach-Zender modulator. The optical beam passes through an acousto-optical (AO) deflector, deflecting the beam to various points on the target. An AO deflector was chosen to allow for very precise steering of the beam under a wide variety of conditions while still being very repeatable.

The beam then returns to an optical detector that converts the modulated optical beam into RF power. The phase of this returned measurement

arm signal beam is compared with that of the reference beam using a telecommunications "IQ" demodulator. The phase can be measured very precisely using this method. The difference in the number of RF phase cycles between the reference and the signal can be determined by changing to a slightly different frequency and using a simple linear equation. The "measurement resolution" can be very precise using this method.

An example of a scan across three gauge blocks arranged in a stairstep fashion is shown in Figure 2.

We are pursuing higher precision and accuracy during the next fiscal year. We are also planning on testing the system on several different applications that have high importance to the missions of LLNL.

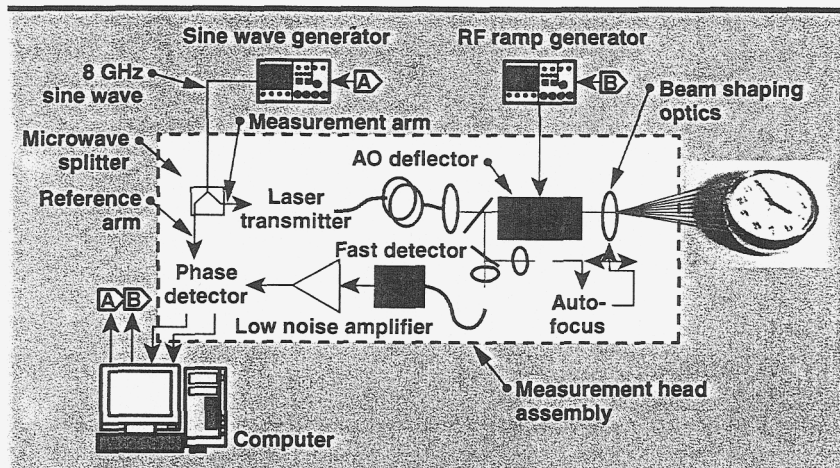


Figure 1. Three-dimensional optical profilometer system showing the system components.

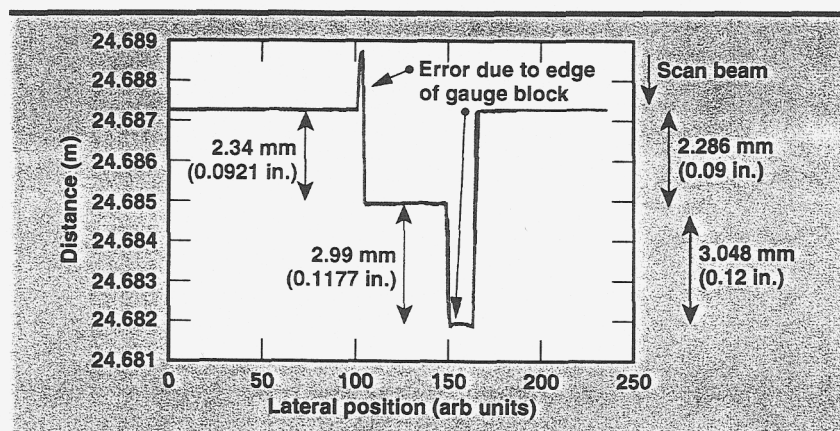
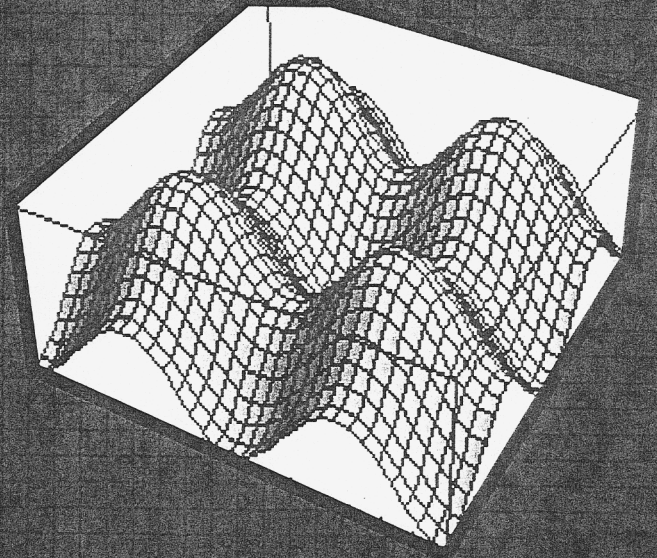


Figure 2. A scan across three gauge blocks arranged in a stairstep pattern.

Center for Precision Engineering



Engineering
Engineering
Engineering
Engineering

mc

Engineering Mesoscale Initiative

D. Meeker, R. Mariella, Jr., H. Louis

The Engineering Directorate's Mesoscale Initiative has as its goal the development of capabilities needed to fabricate target assemblies for the Defense and Nuclear Technologies High-Energy-Density Experimental Science (HEDES) Program. Many of these targets will be fielded on the Omega and National Ignition Facility (NIF) lasers, and a number of these targets will require surface finishes in the 50-to 100-nm range, and surface features approaching 1 μm . We are coordinating efforts to ensure that the proper capabilities are being developed, and performing feasibility studies of new approaches to yield the needed capabilities.

The HEDES share of the NIF shot schedule amounts to 200 to 300 shots a year. Of that number, we estimate that 80% to 90% of the targets can be produced with extensions to existing capabilities; the Mesoscale Initiative is focused on the more difficult targets remaining. Therefore, a successful Mesoscale Initiative will result in a capability that can produce this wide range of targets in sufficient numbers.

Targets could have planar, cylindrical, or spherical geometries, in materials that vary from very-low-density foams such as aerogels, to high-density, high-Z shells serving as high-pressure fuel capsules. The targets could have 1-, 2-, or 3-D features on their surfaces, with feature size in the μm to tens of μm range.

To reach that end, we are coordinating various research and technology efforts to ensure that the proper capabilities are being developed, and to do feasibility studies of new approaches to yield these capabilities. Finally, the Initiative is responsible for coordinating Engineering's efforts with those of the NIF Ignition Target Fabrication Group, and for keeping Engineering management aware of requirements and progress.

Fabricating these targets is just part of the process. Once fabricated, the targets, which are usually made up of several components, must be assembled and characterized. Thus, the Initiative has six elements: material synthesis; material removal; material deposition; metrology of components; assembly; and characterization of the assembly. This year, the project focused on gathering requirements from the experimentalists and theoreticians and initiating several LDRD and TechBase projects in the areas of material removal and characterization.

The gathering of requirements provided a vast range of possible target shapes, materials, and feature size. As many as twenty separate proposals for experiments on NIF and Omega are presently being considered, covering areas as diverse as hydrodynamics (preheat, mix, instabilities); opacity; radiation transport; material strength; and equation-of-state studies.

Materials in these targets range from very low density (~ 0.04 g/cc) plastics, with and without dopant or tracer elements embedded, to high-Z metal capsules used as pressure vessels to contain DT fuel. Some targets require surface finishes of the order of 50 nm rms, while others need 3-D surface features with wavelengths of a few to tens of μm , and a few μm and larger amplitudes. We are told these requirements very likely will change in time, but we can get a pretty good estimate from the present needs. Thus, we will be developing capabilities to machine a few μm to many μm amplitude features with 50-to 100-nm finishes in materials as varied as low density foams to high-Z metals.

In FY01, Engineering successfully proposed three LDRD projects that are critical to the Mesoscale Initiative. The first LDRD project is a continuation of a mid-year proposal to design and build an x-ray microscope capable of characterizing small (~ 1 cm) targets to sub- μm resolution.

A second LDRD is studying the enhancement of a fast servo tool to be added to the z axis of a diamond turning machine. By increasing the speed this tool can move in and out, we can greatly enhance the material removal on complex, 3-D features.

The third LDRD is studying the material removal characteristics of an ultra-short-pulse laser. Here, experiments are coupled to modeling efforts to see if a deterministic behavior can be identified, and if these lasers are capable of delivering the surface finishes required.

During FY02, we are expanding our study to sub- μm accuracy. We also expect to learn from our ultra-short-pulse laser LDRD project the capabilities of femtosecond lasers as tools to machine surfaces to required surface finishes. Our LDRD on the x-ray microscope should be through its design stage and ready for construction. The fast tool servo LDRD is expected to yield results in increasing the repetition rate of the servo when mated to a diamond turning machine. We will also assess the feasibility of adapting FIBEs to a multi-ion, variable current machine that could be used to remove or deposit material.

Fast Tool Servo Application to Single-Point Turning Weapons Physics Targets

R. C. Montesanti, D. L. Trumper (MIT), J. L. Klingmann

High-Energy-Density Experiments play an important role in corroborating the improved physics codes that underlie LLNL's Stockpile Stewardship mission. Conducting these experiments presently on Omega at Rochester, and in the future on NIF, requires improving the fabrication capability for the target assemblies. These targets are mm-sized assemblies of components with μm -sized features. A faithful mapping of experiment to computer simulation requires an ability to produce parts with a high surface contour accuracy and low surface roughness.

Single-point diamond turning is currently the best method for a high material removal rate with non-iterative accuracy and low surface roughness. Current single-point turning can handle only special cases of contoured surfaces. New experiments for Stockpile Stewardship require surfaces that exceed LLNL's current single-point fabrication capability. The two-directional sinusoidal surface shown in Figure 1 is one example.

Single-point turning requires the tool to accurately follow a rapidly changing trajectory as the workpiece passes by. A fast tool servo (FTS) is a small, fast-moving machine axis that can be added to a single-point turning machine to accomplish this.

The goal of this project is the improvement of a 100-Hz bandwidth commercial FTS, shown in Figure 2, that LLNL purchased in FY00. Preliminary work at LLNL indicated that this FTS did not perform as anticipated, and would severely limit the fabrication process by requiring extremely low spindle rotation speeds.

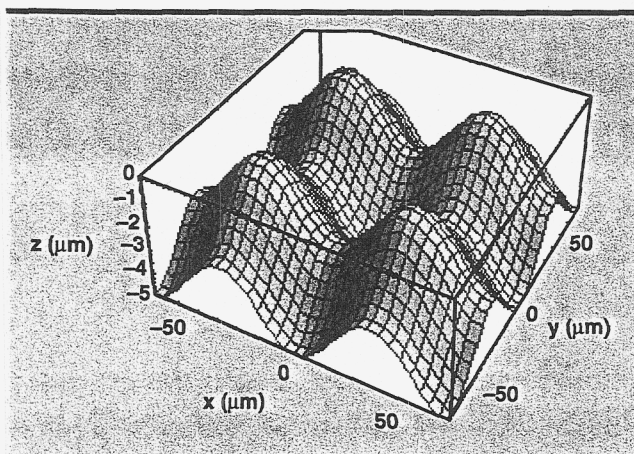


Figure 1. Example of a desired two-directional sinusoidal surface, 70- μm spacing, 5- μm height.

During FY01 the FTS was shipped to the Precision Motion Control Laboratory at MIT to become part of the work being conducted there. The initial assessment at MIT was that the FTS controller is embedded within the proprietary circuit boards of the system, making it impractical to directly modify the controller behavior. We decided instead to treat the entire system (mechanical and proprietary controller) as the plant (a dynamic sub-system), and plan to wrap a compensating loop around it, using a Simulink-based controller implemented on a dSpace controller card.

Preparation for this work was accomplished by a re-commissioning effort on a two-axis diamond turning machine at MIT; the FTS will be integrated with this for cutting tests. Specifically, the electrical, electronic, and control systems for the machine were modified and updated to allow integration of a dSpace control system, and safe operation of the machine.

During FY02 we will complete the following:

1. Measure the step response of the FTS amplifiers;
2. Measure the step response of FTS position feedback device;
3. Characterize the open-loop response of the FTS;
4. Measure the closed-loop response of the FTS;
5. Design the outer loop controller using Simulink;
6. Implement the controller using dSpace;
7. Integrate the FTS with the MIT diamond turning machine and produce a test part.

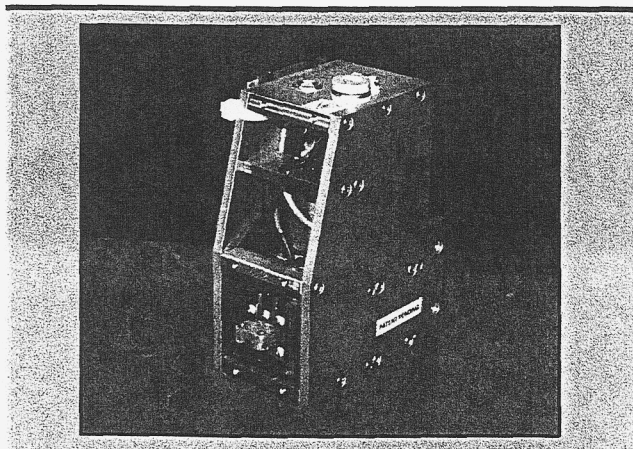
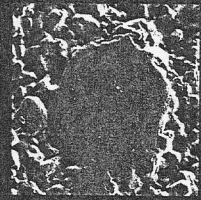
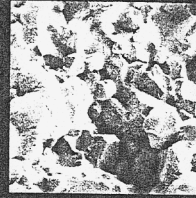
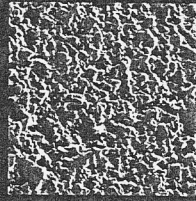


Figure 2. 100-Hz commercial fast tool servo owned by LLNL.

Other Technologies



ENGINEERING
ENGINEERING
ENGINEERING

mm

Frame Extraction and Image Processing in Scene Analysis

A. Gooden, L. Scott

This project has two phases: first, to determine an effective and efficient method for frame extraction from an MPEG-2 video stream; second, to apply image processing techniques to the frames for the enhancement of images for artificial neural network processing.

This real-time scene analysis project consists of a series of modules connecting several components, including a smart camera system, frame extraction and image processing software, and neural networks. The camera will capture video streams, which will be broken into sets of frames that will be manipulated by image processing algorithms. Neural networks will be added to produce a system by which objects can be identified from remote locations.

As the video is streamed over the network, software captures and decodes the stream, allows the stream to be viewed on the viewer system, controls the camera over the network, and can capture single frames from the stream or record a video loop instead. This software is upgradeable and can trigger alarms remotely, and will be used to send video information to neural network systems, or to image processing modules. The software is one of the image acquisition, control, and transmission components.

Part two of this system consists of components that will be useful in image processing applications. These software packages are customized for use in file type conversion, image compression, frame extraction, automation, filtering, and pattern recognition. The long-term goal is to create modules that will be used in conjunction with existing software for advanced image processing of files retrieved from part one—data acquisition.

It is proposed that this part of the system serve as the mediator between the acquisition system and the neural network. This part will not only prepare the acquired images for the network, but also remove detected blockages and send audio extractions.

The design and implementation of neural networks is part three of this system. The neural networks will decipher images captured by the smart camera and categorize the predetermined objects within the image frame. This is done by implementing learning algorithms on the neural networks.

A neural network is a collection of nodes that emulates neurons in a human brain. Human learning

involves adjustments to the synaptic connections between neurons. This is also how the neural network works. Learning usually occurs by example through training where some algorithm repeatedly adjusts the connection weights. These connection weights store the knowledge necessary to solve specific problems.

Today, neural networks are being applied to an increasing number of complex problems in the world. They are good pattern recognition tools and very effective categorizers. They have the ability to generalize in making decisions about inaccurate data, and offer hypothetical solutions to a variety of classification problems such as speech, and character and signal recognition. The advantage of neural networks lies in their resilience against distortions in the input data and their capability to learn.

The second phase of the project is to apply image processing techniques. Image processing is the manipulation of images by restoring degradation, enhancing appearance, and extracting features. Three major types of image processing techniques were applied: sharpening filters, edge detection, and object removal.

The input of this research was streaming MPEG-2 video. Each video averages one minute. The videos were broken into frames and put into sets. There were 41 sets; each set contained 1800 frames. These frames were used in Stuttgart Neural Network Simulator back propagation and clustering algorithms for training and testing the network. The color single frames were converted to 8-b monochrome bitmap images. The grayscale images were run through the mentioned algorithms. Each algorithm was used to enhance the images.

More time is needed to teach the neural network different image patterns. This will allow one to see what type of image patterns the neural network can use for better generalization. Time is also needed to produce programs to give a statistical analysis of the neural network, as well as training the neural network more efficiently. It has been proven that it is feasible for the neural network to differentiate and identify objects using visual data. The system as a whole will capture a scene using the CCD camera, extract frames, manipulate the data, and analyze the data using the neural networks.

Once the system is functional, it will provide LLNL with a tool that can be used for surveillance or many other applications.

Surface and Volumetric Flaw Distribution in Brittle Materials

R. A. Riddle, C. K. Syn, S. Duffy, J. Palko, E. Baker (Connecticut Reserve Technologies)

Materials are called "brittle" when their failure involves very little plastic deformation and widely variable failure strengths—glasses and ceramics are two very different examples. Critical applied stresses, i.e., those that cause failure, depend on the size of the flaws, the orientation of the flaws in the material with respect to the applied loads, and the flaw growth resistance of the material. We have previously fabricated and tested a set of flexure specimens taken from an oxide ceramic component. This year we have microscopically examined the failure surfaces to characterize the critical flaws.

When the size and orientation of the flaws in components are unknown, statistical methods are used to predict the adequacy of structural components to survive or to have a certain lifetime under applied loads. Statistical methods are often used with brittle materials because the low fracture toughness of the materials implies that the critical flaws are very small, and hence undetected. Critical flaw sizes for brittle materials are often on the order of a few microns.

Weibull statistics is the most common statistical method applied to the prediction of strength in brittle materials, with two- and three-parameter Weibull

distributions used to correlate probability of failure with stress. A differentiation is made, depending on whether the flaws are distributed randomly throughout the volume of the material, or the defects are restricted to surfaces.

With few exceptions, surface flaws produced by machining or handling are the predominant source of failure in glass. In contrast, ceramic materials have flaw distributions characterized by the presence of both volumetric and surface flaws. When failure data is grouped according to whether the specimen critical flaw was on the surface or within the volume, it is said to be censored.

The location of the critical flaw in a broken specimen, and whether it was a surface or volume flaw, must be determined by microscopic examination of the failure surface. This year we have microscopically examined the failure surfaces to characterize the critical flaws of flexure specimens taken from an oxide ceramic component (Figure 1).

We have developed algorithms implemented in the computer program WeibPar to develop two- and three-parameter Weibull distributions to correlate to the censored data. The values of the Weibull parameters derived are very sensitive to the details of the data partitioning. (See Figure 2 for an example.)

The Weibull parameters thus derived are readily used to predict the reliability of structures analyzed using finite-element analysis. In previous years, LLNL finite-element codes were modified to perform reliability analysis on material with volumetrically distributed flaws. This year, both NIKE2D and NIKE3D were modified to offer reliability analysis for material with surface flaws as well.

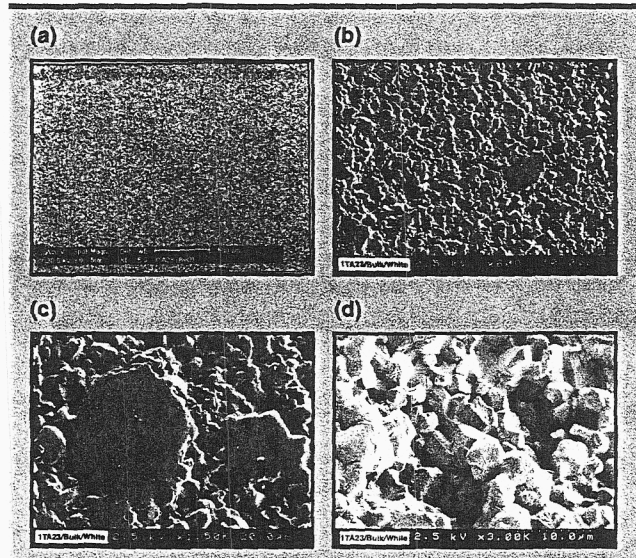


Figure 1. Specimen from low-density white area. (a) Low-magnification micrograph indicating presence of oversized powder grains, shown as black particles. (b) Cross-sectional view, indicating presence of internal porosity. (c) Large particles. Scratch marks on the left particle indicate that it was polished, while the surrounding small particles were crumbling during the polishing. (d) Enlarged view of two porosities in (b).

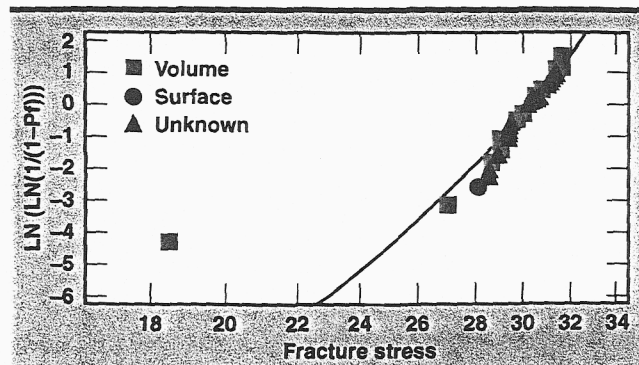


Figure 2. Cumulative Weibull distribution line. The data set has been censored according to flaws found on the surface of the specimen and within the volume.

Nitrogen Augmentation Combustion Systems

L. E. Fischer, B. Anderson

This work combines multi-stage combustion technology with nitrogen-enriched air technology to 1) control the combustion temperature and products; 2) extend the maintenance and lifetime cycles of materials in contact with combustion products; and 3) reduce pollutants, while maintaining relatively high combustion and thermal cycle efficiencies.

Increasing fuel efficiency in combustion engines, while simultaneously reducing polluting exhaust emissions, has been researched over the past 25 years and subsidized by the federal government.

Maximum fuel efficiency normally occurs at or near stoichiometric conditions, where the fuel is completely oxidized. In practice, the combustion process in an engine is usually with air and not with pure oxygen. When oxygen is supplied by dry air, 3.76 moles of nitrogen will accompany one mole of oxygen. The stoichiometric air-fuel ratio is the ratio of the mass of air to the mass of fuel to result in stoichiometric combustion. The actual operating condition of an engine is usually expressed in terms of the equivalence ratio, which is the ratio of the stoichiometric air-fuel ratio to the actual air-fuel ratio. The equivalence ratio is 1.0 when the engine is operating at stoichiometric conditions.

When an engine operates at an equivalence ratio greater than 1.0, it is operating fuel-rich and produces pollutants such as hydrocarbons (HC), carbon monoxide (CO) and particulate matter. At equivalence ratios less than 1.0, the engine produces oxides of nitrogen (NO_x), which are a major source of photochemical smog, and are regulated. Also the combustion gases can be very corrosive with the excess oxygen, and can reduce the life of the engine.

This TechBase work combines multi-stage combustion technology with nitrogen-enriched air technology to control the combustion temperature and products. The first stage of combustion operates fuel-rich, where most of the heat of combustion is released by burning it with nitrogen-enriched air. Part of the energy from the

combustion gases is used to perform work or to provide heat. The cooled combustion gases are reheated by additional stages of combustion until the last stage is at or near stoichiometric conditions, and additional energy is extracted from each stage to result in relatively high thermal cycle efficiency. The air is enriched with nitrogen using air separation technologies such as diffusion, permeable membrane, absorption, and cryogenics.

Our computer modeling has indicated that the use of multi-staged combustion coupled with nitrogen-enriched air could result in extremely low NO_x pollution levels and still achieve relatively high combustion efficiency. Two white papers were written documenting the computer modeling and results, one on gas turbine performance and the other on coal burning systems. In both cases the NO_x was reduced by two orders of magnitude and the free oxygen by two to three orders.

Potential industrial partners, such as OEMs for power production, OEMs for NO_x sensors and control systems, and the EPA have been contacted to gauge the level of interest in this technology. Two OEMs for power production—GE Turbines and ABB Power Systems—along with Marathon Sensors and the EPA have also indicated interest in this technology. Contacts are being developed with OEMs for nitrogen-enrichment processes. A provisional patent on this new technology has been filed to allow open discussions with industry.

Staged Combustion with Nitrogen-Enriched Air (SCNEA) development was originally funded in FY01 as a technology base project. SCNEA is viewed as a possible alternative combustion technology for stationary combustion processes such as boilers, furnaces, and gas turbines. SCNEA can be implemented relatively easily in coal-burning power plants that already use two-staged combustion to lower NO_x. By enriching the nitrogen in the air to 86% in the first stage of combustion the NO_x can be further reduced by two orders of magnitude. Estimated capital and operational costs for implementing this technology appear to be very competitive.

Author Index

11

Author Index

Anderson, B.	55	Laskowski, G.	19
Ashby, E.	44	Leach, Jr., R. R.	13
Bakajin, O.	35	Lee, C.	13
Baker, E.	54	Lennon, W. J.	7
Barbee, T.	41	Lewis, P.	4
Bernhardt, A. F.	31	Lin, J.	22
Bodtker, B.	7	Loomis, M.	18
Bond, T. C.	33	Louis, H.	49
Bowers, M. W.	46	Maghribi, M.	29
Brase, J.	8	Malba, V.	31
Brewer, L. R.	35	Mariella, Jr., R.	30, 49
Carrano, C.	8	McCallen, D. B.	4
Ciarlo, D. R.	36, 44	McCallen, R.	19
Colon, D.	7	McConaghy, C.	11
Cooper, G.	34	Meeker, D.	49
Couch, R.	17	Meyer, G.	33
Daily, L.	17	Miles, R. R.	33
Dallum, G.	10	Miller, W. O.	40
De Groot, A.	26	Mish, K.	18
Dolan, K.	42, 45	Montesanti, R. C.	50
Duffy, S.	54	Morse, J. D.	24
Dunn, T.	17, 19	Nederbragt, W.	41
Evans, L.	31	Noble, C. R.	6
Ferencz, R.	21	Palko, J.	54
Fischer, L. E.	55	Perry, R.	42
Flath, L.	5	Pierce, E.	25
Fugina, J.	42	Pocha, M. D.	33
Glaser, R.	20	Poggio, A. J.	3
Gooden, A.	53	Puso, M. A.	23
Graff, T.	34	Raley, N.	34
Harris, D. B.	4, 10	Riddle, R. A.	54
Harvey, C. D.	31	Rikard, R. D.	42
Haskins, J.	42	Roberson, G. P.	39
Haupt, D.	45	Rock, D. W.	4
Havstad, M. A.	24	Romero, K.	9
Henderer, B.	13	Rose, K.	35
Hernandez, J. E.	10	Rusnak, B.	43
Hinkling, T.	20	Sanders, D.	32
Hoover, C.	21, 26	Sanford, L.	25
Hurd, R.	5	Sawvel, R.	5
Johnson, G. W.	46	Schaich, P. C.	39
Jones, H. E.	39	Schneberk, D.	41, 45
Kallman, J.	44	Scott, L.	53
Kartz, M. W.	39	Shapiro, A.	21
Kinney, J.	45	Sharpe, R. M.	18
Klingmann, J. L.	41, 50	Sherwood, R.	26
Kruevitch, P.	29, 35	Sicherman, A.	20
Lamont, A.	20	Speck, D.	25
Lane, S.	41	Stewart, J.	20

Author Index (continued)

Swift, D. W.	46	Trumper, D. L.	50
Syn, C. K.	54	Woehrl, T.	12
Thigpen, R.	41	Wolfe, J.	32
Thomas, G.	44	Zumstein, J.	9
Thompson, C. A.	5		

Manuscript Date September 2002
Distribution Category UC-42

This report has been reproduced directly from the best available copy.

Available to DOE and DOE contractors from the
Office of Scientific and Technical Information
P.O. Box 62, Oak Ridge, TN 37831
Prices available from (423) 576-8401
<http://www.osti.gov/bridge/>

Available to the public from the
National Technical Information Service
U.S. Department of Commerce
5285 Port Royal Rd.
Springfield, VA 22161
<http://www.ntis.gov/>

OR

Lawrence Livermore National Laboratory
Technical Information Department's Digital Library
<http://www.llnl.gov/tid/Library.html>

This document was prepared as an account of work sponsored by an agency of the United States Government. Neither the United States Government nor the University of California nor any of their employees, makes any warranty, express or implied, or assumes any legal liability or responsibility for the accuracy, completeness, or usefulness of any information, apparatus, product, or process disclosed, or represents that its use would not infringe privately owned rights. Reference herein to any specific commercial products, process, or service by trade name, trademark, manufacturer, or otherwise, does not necessarily constitute or imply its endorsement, recommendation, or favoring by the United States Government or the University of California. The views and opinions of authors expressed herein do not necessarily state or reflect those of the United States Government or the University of California, and shall not be used for advertising or product endorsement purposes.

Work performed under the auspices of the U.S. Department of Energy by the University of California, Lawrence Livermore National Laboratory under Contract W-7405-Eng-48.
ENG-01-0043b-AD

Techn
Techn
Techn
Techn



Engineering Directorate
Lawrence Livermore National Laboratory
University of California
P.O. Box 808, L-124
Livermore, California 94551

<http://www-eng.llnl.gov/>

me